

https://dspace.org/

MeerKAT discovery of an infalling cold gas tail on to the nearby barred spiral galaxy NGC 5643

Karina Santana; Filippo M. Maccagni; Julia Healy; Roger Deane

OXFORD UNIV PRESS
https://hdl.handle.net/10539/46011
WOS

Downloaded from a DSpace repository. https://dspace.org/

Monthly Notices of the ROYAL ASTRONOMICAL SOCIETY

MNRAS **540,** 2396–2412 (2025) https://doi.org/10.1093/mnras/staf832
Advance Access publication 2025 May 23

MeerKAT discovery of an infalling cold gas tail on to the nearby barred spiral galaxy, NGC 5643

Karina C. Santana [1]★ Filippo M. Maccagni [2] Roger P. Deane [1,3] and Julia Healy [4,5]

[1] *Wits Centre for Astrophysics, School of Physics, University of the Witwatersrand, 1 Jan Smuts Avenue, 2000, Johannesburg, South Africa*
[2] *INAF – Osservatorio Astronomico di Cagliari, via della Scienza 5, I-09047 Selargius, CA, Italy*
[3] *Department of Physics, University of Pretoria, Hatfield, Pretoria 0028, South Africa*
[4] *Jodrell Bank Centre for Astrophysics, School of Physics and Astronomy, University of Manchester, Oxford Road, Manchester M13 9PL, UK*
[5] *United Kingdom SKA Regional Centre (UKSRC), University of Manchester, Oxford Road, Manchester M13 9PL, UK*

Accepted 2025 May 15. Received 2025 May 13; in original form 2024 November 22

ABSTRACT

The detailed study of gas flows in local active galactic nuclei (AGN) is essential for understanding the regulation of star formation and black hole growth, which are fundamental to galaxy evolution. One such AGN case study is NGC 5643, a nearby ($D_L \sim 17.3$ Mpc) star-forming, late-type, Seyfert galaxy, where inflows and outflows have been observed in detail. NGC 5643 has been studied at multiple wavelengths; however, a key missing component is sensitive, high-resolution neutral hydrogen (H I) observations. We present 21-cm observations of NGC 5643 with MeerKAT, revealing six low-H I mass ($M_{\rm H\,I} \sim 10^7$ M$_\odot$) sources surrounding NGC 5643 and H I in IC 4444, $\sim$ 230 kpc north of NGC 5643. In NGC 5643, H I extends beyond the stellar disc with several morphological and kinematical asymmetries. North of the disc is an extended 30 kpc tail with counterrotating velocities. This is H I gas accreting on to the regularly rotating disc of NGC 5643 from the environment. Within the spiral arms of the disc, we identify extraplanar gas components, tracing galactic fountains driven by star formation regions. These fountains have a molecular gas component and show an increased H_2/H I ratio. In the circum-nuclear region, we observe spatially unresolved H I absorption that is slightly blue-shifted (~ 72 km s^{-1}) with an H I emission counterpart at red-shifted velocities. These MeerKAT observations provide a complete census of the H I in and around this nearby Seyfert galaxy, providing missing information on the cold gas flows fuelling the star formation and nuclear activity.

Key words: ISM: kinematics and dynamics – galaxies: individual: NGC 5643 – galaxies: ISM – galaxies: Seyfert – galaxies: star formation – radio lines: galaxies.

1 INTRODUCTION

Galaxies are the building blocks of the Universe; their formation and evolution involve a complex interplay of multiple physical processes. The current understanding of galaxy formation suggests that galaxies form from the collapse of primordial gas clouds, which then undergo hierarchical merging and accretion, as well as inflows and outflows (see Press & Schechter 1974; Péroux & Howk 2020; Watkins et al. 2023; and references therein). The processes influencing galaxy evolution can be broadly divided into external environmental processes: mergers, tidal interactions, and hydrodynamical forces such as ram pressure stripping; internal processes: including feedback generated by star formation (SF) and active galactic nuclei (AGN; Hopkins et al. 2016), and slow secular processes such as the redistribution of galactic mass and energy induced by the formation of bars, spiral arms and galactic winds within the disc (Kormendy & Kennicutt 2004). These processes lead to gas entering and being removed from galaxies at different rates and temperatures, thus regulating SF and the accretion of the supermassive black hole (SMBH). This recycling of gas between the galaxy and the environment ultimately regulates the evolution of galaxies (Kereš et al. 2005; Rodríguez Montero et al. 2019).

Understanding how AGN and galactic discs are fuelled is one of the main open questions of galaxy evolution. One way the AGN of a galaxy can be sustained is by halo gas accreting on to the galactic disc. Accretion of gas into galaxies has been traced by the kinematics of the neutral atomic (H I) disc of galaxies (Sancisi et al. 2008), while accretion of gas on to AGN is difficult to trace directly. In the brightest cluster galaxies, molecular clouds and filaments form stars and are believed to feed the SMBH at the centres of these galaxies (Harrison et al. 2018). In Seyfert galaxies, which are typically hosted by star-forming galaxies, H I discs can trace recent accretion (Best & Heckman 2012). We aim to determine whether this accretion can be linked to the triggering of nuclear activity, and if so, which mechanisms are responsible for it. The mechanisms driving accretion involve both external processes, such as gas inflows from the environment, and internal processes such as the redistribution of gas within the galactic disc. These accretion processes can also be influenced by other factors, including galaxy mergers, which can enhance the inflow of gas towards the central AGN.

★ E-mail: kcsantana02@gmail.com

© 2025 The Author(s).
Published by Oxford University Press on behalf of Royal Astronomical Society. This is an Open Access article distributed under the terms of the Creative Commons Attribution License (https://creativecommons.org/licenses/by/4.0/), which permits unrestricted reuse, distribution, and reproduction in any medium, provided the original work is properly cited.

Downloaded from https://academic.oup.com/mnras/article/540/3/2396/8142523 by jamestemlett user on 14 August 2025

Galaxy mergers are one of the most common mechanisms that trigger AGN and account for some of the most luminous AGN (Hopkins et al. 2005; Poggianti et al. 2017, and references therein). When two galaxies merge the rotating gaseous discs of both galaxies are disrupted and mixed, then re-collapse, activating SF and funnelling gas towards the nuclei, thereby fuelling the AGN (Hopkins et al. 2005; Poggianti & GASP Team 2023).

Hydrodynamical interactions such as ram pressure have been connected to gas removal and increased local SF in the outskirts of galaxies (e.g. Poggianti et al. 2017; Ellison, Catinella & Cortese 2018; Radovich et al. 2019). This is usually associated with galaxies in clusters or massive groups where the dense intergalactic medium (IGM) efficiently acts as a drag force on their gaseous discs. As a galaxy moves through these dense environments, the gas in the disc compresses, driving it towards the central SMBH and potentially triggering nuclear activity (Poggianti et al. 2017). Meanwhile, less dense gas, such as H I, is stripped from the galaxy. This stripped gas, having lost its angular momentum, may be pulled back towards the AGN by the galaxy's gravitational potential energy, overcoming the reduced kinetic energy of the gas and possibly triggering the AGN (Poggianti et al. 2017).

Investigating the fuelling of AGN has traditionally been limited to H I absorption studies due to sensitivity limitations of older radio telescopes. A prime example of accretion is seen in NGC 315, where Morganti et al. (2009) used H I absorption kinematics to confirm gas accretion on to the galaxy. They found that the immediate environment of NGC 315 is gas-rich, with one of the absorption features most likely associated with a gas cloud falling into NGC 315. Another example is the study of H I in PKS B1718–649 by Maccagni et al. (2014) which identified H I absorption features associated with two small clouds not regularly rotating with the galaxy. Maccagni et al. (2014) concluded that the AGN in PKS B1718–649 is triggered by local mechanisms, such as accretion of small gas clouds, rather than gas-rich mergers.

In radiatively efficient AGN, accretion on to the SMBH creates a stable accretion disc, and the host galaxies are often associated with SF activity (Best & Heckman 2012). These galaxies, often referred to as Seyfert galaxies, typically emit most of their energy through radiative winds and they often host low-power jets. These jets may have an effect on the surrounding ionized gas (e.g. Mingozzi et al. 2019; Venturi et al. 2021), as well as the molecular and H I gas. IC 5063 is a prime example where the radio jets expanding within the innermost kpc generate a multiphase outflow extending ~ 1 kpc (Morganti et al. 2015). These outflows are detected in molecular gas, H I, and ionized gas (see Morganti, Oosterloo & Tsvetanov 1998; Oosterloo et al. 2000; Morganti et al. 2013; Dasyra et al. 2016, and references therein). This removal of gas may eventually deplete the galaxy of its gas supply and halt SF; a process referred to as negative feedback.

AGN feedback is not limited to the negative feedback effect on SF but can also have a positive feedback effect, enhancing SF. Centaurus A (NGC 5128) is an example where star-forming regions are triggered by the expansion of the radio jets at the outskirts of its stellar body. The radio jets eject but also compress the multiphase gas at the edges of the disc and generate a region of recent SF (Santoro et al. 2016; Salomé et al. 2017). Centaurus A and its outflows have been extensively studied due to the proximity of NGC 5128 (3 Mpc); however, a comprehensive understanding of AGN and stellar feedback and their effects on the evolution of galaxies requires a detailed analysis of a larger sample of nearby AGN and star-forming galaxies. We need both sensitive and high-resolution observations to probe the diffuse environment as well as the small-scale structures of a galaxy.

Table 1. Basic properties of NGC 5643.

Parameter	Value	References
AGN type	Seyfert 2	Morris et al. (1985)
Centre α (J2000)	$14^{h}32^{m}40.56^{s}$	Stuber et al. (2023)
Centre δ (J2000)	$-44^{\circ}10'28.56''$	Stuber et al. (2023)
Inclination ($^{\circ}$)	$27^{\circ} \pm 5^{\circ}$	Morris et al. (1985)
log(SFR [$M_{\odot}yr^{-1}$])	0.39	Pan et al. (2022)
$\log_{10} M_{\star}$ ($M_{\odot}$)	10.34	Leroy et al. (2021)
Optical redshift	0.004	Cresci et al. (2015)
Flux [1.4 GHz] (mJy beam^{-1})	17	This work
Average H I mass ($M_{\odot}$)	4.4×10^{9}	This work

From these studies it is evident that a key component in understanding the feeding and feedback in AGN is the neutral atomic hydrogen (H I) spatial distribution and kinematics. H I gas is fundamental for understanding the processes that drive galaxy formation and evolution as it is a prime ingredient of SF. For the SF process, H I cools and transforms into molecular gas, H_2, collapsing into a denser state (Sancisi et al. 2008). H I has been observed to be involved in fuelling AGN through emission and absorption lines, for example, in NGC 315 (Morganti et al. 2009) and NGC 3100 (Maccagni et al. 2023).

New radio telescopes, such as the South African MeerKAT telescope, offer a larger field of view, improved spatial and spectral sensitivity and are capable of detecting the H I emission line. This allows us to greatly improve our knowledge of H I in nearby AGN with short observing times (for example Maccagni et al. 2021). MAGNHIFFIC.[1] (MeerKAT AGN H I Feeding & Feedback Investigation Close-by) is an ongoing study of the processes of feeding and feedback in nearby AGN ($D < 80$ Mpc) with different energetic outputs, ages, hosts and environments, which leverages sensitive MeerKAT observations of the cold H I to simultaneously probe, for the first time, the small scales near the SMBH, the larger scales of the galactic discs and the environments of these AGN. NGC 5643 is one of the first galaxies observed in this project.

NGC 5643 is a Seyfert galaxy where positive feedback has been identified. It is a nearby ($D_L = 17.3$ Mpc, 1"$\approx$ 83 pc) barred spiral galaxy, viewed almost face-on (incl $= \sim 27^{\circ} \pm 5^{\circ}$), with the bar oriented in an east–west direction (Cresci et al. 2015). There is a clear dust lane parallel to the southern leading edge towards the east of the bar. The basic properties of NGC 5643 are given in Table 1. NGC 5643 appears to be isolated, with only one other galaxy, PGC 538542, that is known to be in its environment (Kourkchi & Tully 2017). The redshift of PGC 538542 is $0.0036 \pm 1.5 \times 10^{-4}$, which is similar to NGC 5643 (Jones et al. 2009).

NGC 5643 has been extensively studied across the electromagnetic spectrum. In the nucleus of NGC 5643, there is strong extended line emission from ionized gas which is traced by [O III] cones extending ~ 1.6 kpc along the bar, observed with MUSE (Cresci et al. 2015). These double-sided ionization [O III] cones show that the central region has out-flowing ionized gas, which is blue-shifted with a projected velocity out to ~ 450 km s^{-1}. These outflows point towards star-forming clumps 5 and 10 arcmin east of the nucleus. Cresci et al. (2015) suggest that this is due to positive feedback from

[1] https://magnhiffic.astron.nl

Downloaded from https://academic.oup.com/mnras/article/540/3/2396/8142523 by jamestemlett user on 14 August 2025

these outflows, implying that positive feedback may be an important mechanism in this galaxy.

The radio structure of NGC 5643 was observed with the Very Large Array (VLA) and reported by Morris et al. (1985) at 1.5 GHz, who note the radio emission is aligned with the bar of the galaxy and extends over ~ 1.6 arcmin . Leipski et al. (2006) also report on VLA radio continuum images, but with greater sensitivity, and find that NGC 5643 has two weak, uncollimated, radio jets on either side of the nucleus, which are ~ 30 arcsec long with radio luminosity, $vL_v\,[8.4\,\mathrm{GHz}] = 0.55 \times 10^{13}$ W (Leipski et al. 2006).

Observations made with the Atacama Large Millimeter/submillimeter Array (ALMA) of NGC 5643 show that the molecular CO $(2-1)$ gas disc extends a few hundred parsecs in size surrounding the AGN and is oriented in a north–south direction (Alonso-Herrero et al. 2018). The kinematics of the rotating disc appears to be at a different position angle (PA) and inclination compared to the large-scale disc. The estimated total molecular gas mass of the nuclear disc and the AGN is $M_{H_2} = 1.1 \times 10^7$ $M_\odot$. Alonso-Herrero et al. (2018) also questions a region of cleared gas in the east which may be associated with a sub-kpc jet, however, there is insufficient evidence to support this assumption.

NGC 5643 is part of the large Physics at High Angular resolution in Nearby GalaxieS survey (PHANGS; Leroy et al. 2021). The PHANGS survey observed a sample of 90 of the nearest, most massive and star-forming galaxies accessible with ALMA, forming the PHANGSS-ALMA survey which Pan et al. (2022) reports on. NGC 5643 is one of these galaxies, with a significant offset (0.4 dex) from the star-forming main sequence and shows relatively high ($\gtrsim$50 per cent) CO fractions in the ALMA field of view (Pan et al. 2022). They find that the CO follows the stellar galactic structures well, which, in the case of NGC 5643, is a barred spiral, suggesting a dynamic origin of these fractions.

Even though NGC 5643 has been extensively studied at multiple wavelengths, the role of H I in this galaxy is poorly constrained. Only the H I Parkes All-Sky Survey (HIPASS; Barnes et al. 2001; Meyer et al. 2004) integrated H I flux ($S_{int} = 56.5 \pm 4.7$ Jy km s^{-1}) is available, and due to the HIPASS resolution of 15 arcmin, the source is unresolved, preventing detailed studies on the circumnuclear regions (see Koribalski et al. 2004; Meyer et al. 2004). To address this limitation, we conducted 21-cm MeerKAT observations of NGC 5643 that span from the circumnuclear region near the AGN to the outer regions of the galaxy. These observations aim to provide insight into the mechanisms fuelling the AGN and the broader feedback process in NGC 5643.

In this paper we present deep H I MeerKAT observation in combination with deep optical observations which, for the first time characterize the H I distribution in this nearby Seyfert galaxy as well as its satellites. In Section 2, we describe our observations, calibration, source finding and the ancillary data used in this paper. In Section 3, we present our results on H I in and around NGC 5643. Section 4 discusses the physical interpretation of our results and compares them to similar findings. The conclusions are presented in Section 5. Throughout this paper, we assume ΛCDM (Lambda cold dark matter) cosmology with cosmological constants values of $H_0 = 70$ km s^{-1} Mpc^{-1}, $\Omega_\Lambda = 0.7$ and $\Omega_M = 0.3$. At the distance of NGC 5643, 1arcsec is 83 pc in the image space.

2 OBSERVATIONS AND DATA REDUCTION

In this section, we describe the observations, data and data reduction techniques used in this study. We utilize MeerKAT *L*-band observations to image and analyse the H I in NGC 5643, along with deep optical observations from the VLT Survey Telescope (VST) to identify any optical counterpart to the H I features.

2.1 MeerKAT *L*-Band observations

The MeerKAT observations of NGC 5643 were conducted at night on 2021-03-19 and 2021-06-05 (SCI-20210212-FM-01, PI Maccagni) in two separate 5.5-h tracks. The target was observed while rising and setting to maximize coverage of the *uv*-plane. Here, we present the observations in the frequency range $1340.0 - 1444.5$ MHz at the original spectral resolution of (26.12 kHz).

The observations were processed with the Containerized Automated Radio Astronomy Calibration (`CARACal`) pipeline (Józsa et al. 2020), which is a Python-based, containerized pipeline commonly used for the reduction of MeerKAT continuum and H I observations (e.g. Maccagni et al. 2020; Namumba et al. 2021; Ianjamasimanana et al. 2022; Serra et al. 2023; de Blok et al. 2024). The data reduction strategy follows that of the MeerKAT Large Survey programmes, MeerKAT Fornax Survey (Serra et al. 2023) and MHONGOOSE (de Blok et al. 2024), to which we refer for a detailed description. Here, we briefly summarize the three main stages of the process: cross-calibration, self-calibration, and spectral-line imaging.

In the first stage, we calibrated the single 5.5-h tracks independently. After cross-calibration of the target, the single tracks were flagged for radio frequency interference through automated AOflagger routines (Offringa, van de Gronde & Roerdink 2012) and self-calibrated using `wsclean` (Offringa et al. 2014) and `cubical` (Kenyon et al. 2018). Self-calibration was performed over the full 100 MHz band divided in four spectral bins. The self-calibration solutions were then transferred to the measurement sets at the original spectral resolution using `crystalball`. The continuum model was then subtracted from the measurement sets, and additional continuum subtraction was performed by fitting and subtracting a first-order polynomial to each point in the *uv*-plane independently (excluding the spectral range of known H I emission). A last flagging routine was then run to remove the residual broad-band RFI typical of the short baselines of interferometers near $u = 0$ (Hess et al. 2015; Carignan et al. 2016; Heald et al. 2016; Maccagni et al. 2020).

In the second stage, we jointly deconvolved and self-calibrated the two tracks together to produce the most sensitive 100 MHz continuum image of the galaxy and the 2000 km s^{-1}-wide multiscale H I data cubes.

The final stage involved combining the continuum-subtracted measurement set to generate the data cubes, with a 5.5 km s^{-1} channel width and at multiple resolutions. These resolutions were produced using different Briggs robust weighting values and, in some cases, applying *uv*-tapering, see Table 2. For the purpose of this paper, we focus on three spectral cubes with resolutions of 96, 30, and 8 arcsec, which, at the distance of NGC 5643, correspond to approximately 8.0, 2.5, 0.7 kpc, respectively. These MeerKAT observations are sensitive to column densities of $\sim 10^{18}$, $\sim 10^{19}$, and $\sim 10^{20}$ cm^{-2} for the 96, 30, and 8 arcsec cubes, respectively. Table 2 presents the noise levels in each cube with a channel width of 5.5 km s^{-1}as well as the column density sensitivity, defined at the 3σ level over four channels (~ 20 km s^{-1}), which marks the sensitivity limit of MeerKAT in these observations.

We created these multiresolution cubes to investigate the different features they reveal. The 96 arcsec cube enables us to examine the diffuse gas in the galaxy, while the 8 arcsec cube provides the high resolution required to study the high column density H I in the star-forming disc and H I absorption. The 30 arcsec cube offers a good

Downloaded from https://academic.oup.com/mnras/article/540/3/2396/8142523 by jamestemlett user on 14 August 2025

Table 2. Neutral hydrogen (H I) data cube parameters for three cubes at different angular resolutions, covering a 1.5 deg^2 field of view and a velocity range of approximately 2000 km s^{-1}. The table includes the restoring beam, average channel noise (rms) for a channel width of 20 km s^{-1}, column density sensitivity (3σ over four 5.5 km s^{-1}channels) and pixel size in arcseconds. Also listed are the cleaning parameters used with `wsclean`, including the Briggs robust weighting value and whether *uv*-tapering was applied.

Label	96 (arcsec)	30 (arcsec)	8 (arcsec)
Restoring beam (arcsec)	97 × 95	35 × 25	9 × 6
Channel rms (mJy beam^{-1})	0.37	0.18	0.25
N(H I)$_{3\sigma,20\ \mathrm{km\,s^{-1}}}$ ($\times 10^{19}$ cm^{-2})	0.310	1.42	29.5
Pixel size (arcsec)	30	7	2
Robust weighting	1.0	1.5	0.0
uv-tapering	yes	no	no

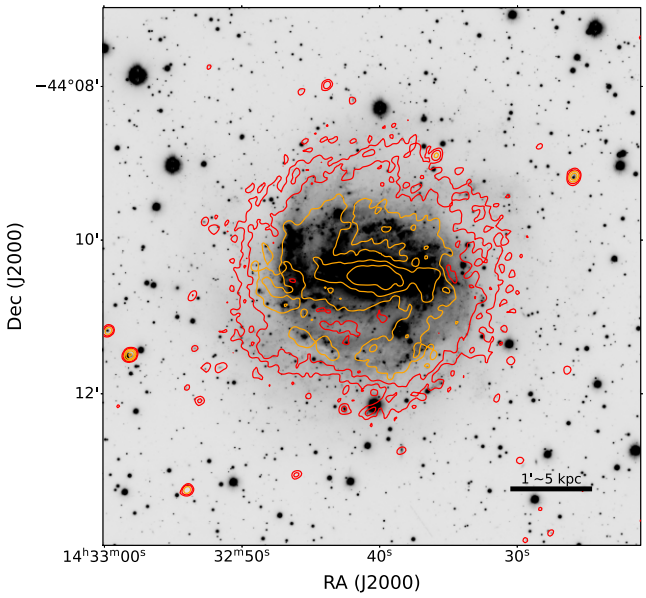


Figure 1. VST *r*-band optical image of NGC 5643 with MeerKAT continuum image contours at $2^n\sigma$ where $n = 2, 3, 4, 5, 6$ and $\sigma = 1.32 \times 10^{-5}$ Jy beam^{-1}. The inner contours (where $n = 4, 5, 6$) are shown in orange to highlight the bar and spiral arm features of NGC 5643 visible in the continuum data. The restoring beam of the MeerKAT continuum image is 6.1 arcsec × 5.0 arcsec with a major axis PA of −42°. The spatial scale is 1.5 arcsec pixel^{-1}.

balance between capturing diffuse gas and resolving high-resolution features and is therefore used for most of the analysis in this paper.

The 1.4 GHz MeerKAT continuum image of NGC 5643 is shown in Fig. 1, overlaid in red and orange contours on the optical VST image. The continuum image has a bandwidth of 100 MHz and an rms noise level of 0.13 μJy. At a resolution of 5.5 arcsec (∼ 0.5 kpc), the radio continuum emission traces the star-forming disc, central bar and the spiral outer arms. The orange contours in Fig. 1 emphasize the central bar and spiral arms in NGC 5643.

2.2 Source Finding

We manually searched the three data cubes for H I sources and identified seven H I detections within the 1.5 deg^2 field of view surrounding NGC 5643. Among these surrounding sources, H I has only been detected in IC 4444, with a HIPASS integrated flux of $S_{int} = 24.9 \pm 3.0$ (Koribalski et al. 2004). To verify the validity of the newly identified sources, we used the automated Source Finding Application (`SoFiA-2`; Westmeier et al. 2021). `SoFiA-2` constructs a source mask by using a smooth and clip (S+C) algorithm, which works by smoothing the data cube on multiple user-defined scales. We set the source detection threshold to signal-to-noise ratio (SNR) of 4. This multiscale smoothing and clipping method is capable of identifying relatively faint and extended features that may have been missed by visual inspection or by applying a single threshold cut-off.

For the automated source finder, we applied the same `SoFiA-2` parameters across all cubes, with the exception of the reliability parameter, which was set to 80 per cent, 75 per cent, and 70 per cent for the 96, 30, and 8 arcsec cube, respectively. The reliability threshold was lowered to include a few visually identified sources that were not automatically detected but have an optical counterpart (see Section 2.3).

We generated the flux density, velocity field and velocity distribution maps of the H I detected within the field. Fig. 2 presents these detections overlaid on the VST *g*-band, optical image (described below). We characterized the H I properties of the detected sources and summarized them in Table 3.

2.3 Optical observations

Assessing the presence of low-surface-brightness galaxies or stellar features associated with the H I emission or absorption detected by MeerKAT requires deep optical observations. As part of the MAGNHIFFIC project, we are collecting sensitive optical data for our targets, either from the Dark Energy CAmera Legacy Survey (DR10-DeCALS), where available, or through targeted observations with the VLT Survey Telescope (VST).

The field of view of the VST-OmegaCAM closely matches that of MeerKAT, covering approximately 1 deg^2, and allows for rapid imaging down to a deep surface brightness limit of 27 mag arcsec^{-2}. This depth is crucial for identifying optical counterparts to the detected H I and for detecting pristine H I clouds. The combination of deep MeerKAT and VST observations, whether from the Fornax Deep Survey (Iodice et al. 2016; Venhola et al. 2019) or from VEGAS (Capaccioli et al. 2015; Spavone et al. 2017), has been instrumental in studying the environment of nearby AGN, such as Fornax A (Kleiner et al. 2021) and NGC 3100 (Maccagni et al. 2023). These datasets have also enabled the discovery of the lowest gas-mass surface brightness galaxy beyond the Local Group (Maccagni et al. 2024).

NGC 5643 was observed with the VST in the *g* and *r* band in April 2024 (project P114, PI Maccagni). A zoomed-in *r*-band image of the target is shown in Fig. 1, while the full-field image, used to identify the sources within ∼1 deg^2 of NGC 5643, is presented in Fig. 2.

2.4 Ancillary data

NGC 5643 has been extensively studied across multiple wavelengths by several surveys. It is part of the PHANGS sample and has been observed with ALMA (Leroy et al. 2021). The ALMA data are available from Canadian Astronomy Data Center (CADC).[2] In this paper, we consider ALMA observations of low-J carbon monoxide, CO(2–1), which trace molecular hydrogen, H_2, throughout the star-forming disc (see e.g. Leroy et al. 2021). Molecular gas in NGC 5643

[2]https://www.canfar.net/storage/list/phangs/RELEASES/PHANGS-ALMA/

Downloaded from https://academic.oup.com/mnras/article/540/3/2396/8142523 by jamestemlett user on 14 August 2025

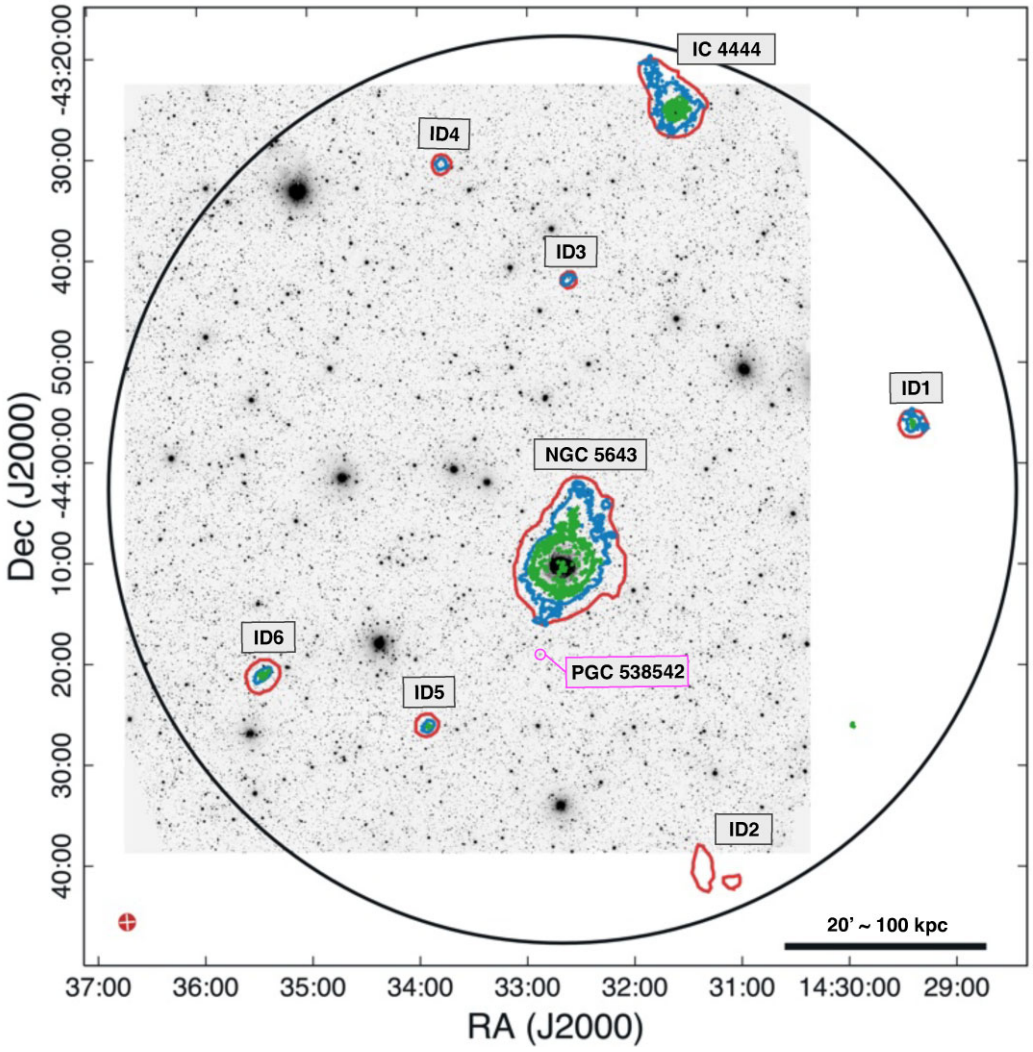


Figure 2. Optical *g*-band VST image of NGC 5643 with H I column density contours (3σ over four channels) at [3.1×10^{18}, 1.4×10^{19}, 2.9×10^{20}] cm^{-2} for each cube with resolution 96 arcsec (outer, red), 30 arcsec (middle, blue), and 8 arcsec (inner, green), respectively. The surrounding sources (excluding IC 4444) are detected for the first time with these H I observations. The closest H I cloud to NGC 5643 is ID5, which is $\sim$ 100 kpc away. The total image area of the MeerKAT observation is enclosed in a 1.5 degree diameter black circle. The beam for the 96 arcsec cube is shown as a red ellipses in the bottom left. The only previously known galaxy in the environment of NGC 5643 is PGC 538542, which is highlighted in magenta.

Table 3. Information on the H I sources within the 1.5 deg^2 field of view from the `SoFiA-2` catalogue and our calculations. In the first column, the newly detected sources are named according to the MeerKAT naming system. The second column provides the shorthand notation for the new sources, as used throughout the paper. The table includes the coordinates of each source, along with the separation, which represents the spatial distance of the sources from NGC 5643. The velocity difference (Δv) is given with respect to NGC 5643, based on the radial velocity $v_{\rm rad}$. The full width at half maximum (FWHM) for each source is listed, including the associated channel width error. The integrated flux ($S_{\rm int}$) was used to calculate the H I masses ($M_{\rm H\,I}$) from the 30 arcsec data, with an estimated 10 per cent error.

Name	id	RA_{J2000} (h m s)	Dec_{J2000} (d m s)	Separation (arcmin)	Separation (kpc)	$v_{\rm rad}$ (km s^{-1})	Δv (km s^{-1})	FWHM (km s^{-1})	$S_{\rm int}$ (Jy km s^{-1})	$M_{\rm H\,I}$ ($\times 10^8 M_\odot$)
MKT J142928.8-435624	ID1	14 29 28.8	−43 56 24	38	189	1137	−55	39 ± 5.5	0.27	0.56 ± 0.06
MKT J143116.7-444045	ID2	14 31 16.8	−44 40 48	34	169	261	−931	16 ± 5.5	0.22	0.37 ± 0.04
IC 4444		14 31 38.4	−43 25 12	47	234	1950	758	165 ± 5.5	3.73	15.3 ± 1.53
MKT J143238.4-434200	ID3	14 32 38.4	−43 42 00	28	139	1898	706	35 ± 5.5	0.09	0.11 ± 0.01
NGC 5643		14 32 40.8	−44 10 12	0	0	1192	0	191 ± 5.5	62.3	43.9 ± 4.39
MKT J143348.0-433036	ID4	14 33 48.0	−43 30 37	41	204	902	−290	25 ± 5.5	0.10	0.28 ± 0.03
MKT J143355.2-442624	ID5	14 33 55.2	−44 26 24	21	105	1923	731	22 ± 5.5	0.13	0.13 ± 0.01
MKT J143526.4-442100	ID6	14 35 26.4	−44 21 00	32	159	822	−310	30 ± 5.5	0.35	0.53 ± 0.05

Downloaded from https://academic.oup.com/mnras/article/540/3/2396/8142523 by jamestemlett user on 14 August 2025

has been detected out to a projected radius of $\sim$ 7 kpc, with an angular resolution of 1.3 arcsec (Leroy et al. 2021).

3 RESULTS

In this section, we present the results from our MeerKAT observations, focusing on the H I in NGC 5643 and its surrounding environment.

3.1 Full field of view

We imaged a 1.5 deg^2 field of view ($\sim$ 448 kpc at D_L = 17 Mpc, the distance of NGC 5643), despite the sensitivity of MeerKAT dropping beyond 1 deg. This larger area was chosen because we detected H I emission from multiple galaxies at the edge of the field of view, allowing for a more complete characterization of their H I properties (see Fig. 2). Only NGC 5643 and IC 4444 have been previously catalogued in H I, the other detections are new and named using the MeerKAT convention, given in Table 3. We assigned numbered IDs to these new detections for brevity in this paper. The contours in Fig. 2 represent the H I column density sensitivity at a 3σ level, assuming a line width of $\sim$ 20 km s^{-1}(four channels) for the 96, 30, and 8 arcsec data cube. The projected spatial separation of the H I sources from NGC 5643 ranges from 21 to 41 arcmin (104 to 206 kpc), while projected velocity separation ranges from 55 to 758 km s^{-1}. The neighbouring galaxy, PGC 538542, as mentioned in Section 1, shows no detectable H I emission. It is likely that the H I in this galaxy has been stripped by the more massive NGC 5643.

H I gas in NGC 5643 is detected in emission (Section 3.2) and absorption (Section 3.3). The H I mass of NGC 5643 is $M_{\rm HI} \approx 4.4 \times 10^9$ M$_\odot$, which is an order of magnitude lower than its stellar mass, $\log(\frac{M_\star}{\rm M_\odot}) = 10.3$ (Leroy et al. 2021). Excluding IC 4444, the surrounding H I sources have an average H I mass of $M_{\rm HI} \approx 3 \times 10^7$ M$_\odot$.

We use the VST image to determine whether these surrounding sources have optical counterparts. The sensitivity of the VST image reaches a surface brightness of $\sim$ 27 mag arcsec^{-2}, allowing us to detect galaxies with stellar masses of 10^6 M$_\odot$. For unresolved sources at the distance of NGC 5643, the brightness limit corresponds to a stellar mass limit of 10^4 M$_\odot$. Therefore at 12 arcsec^2, we obtain a 3σ signal, which constitutes a reliable detection, corresponding to an apparent magnitude of 25.8 and $\log(\frac{M_\star}{\rm M_\odot}) = 4.4$.

When compared to the VST image ID4, ID5, and ID6 have identifiable optical counterparts. The presence of a foreground star makes it difficult to determine whether ID3 has an optical counterpart. ID1 and ID2 fall outside the field of view of the VST image. Further information on these H I sources can be found in the appendix (Fig. A1).

For the first time, we are able to identify these dwarf galaxies and associate them with the environment of NGC 5643 and IC 4444. These discoveries indicate that NGC 5643 is not as isolated as originally thought, which may have implications for its evolution, as explored in this paper.

3.2 H I emission in NGC 5643

Focusing on NGC 5643, we analyse the H I emission using the 96″, 30″ and 8″ data cubes. The integrated flux profile of the 30 arcsec cube (top panel of Fig. 3) traces the H I disc. Additionally, H I absorption is detected in the centre of NGC 5643 (bottom panel of Fig. 3), which we discuss in the next section. The integrated flux profile exhibits a symmetric double-horn shape, tracing the rotation of the disc;

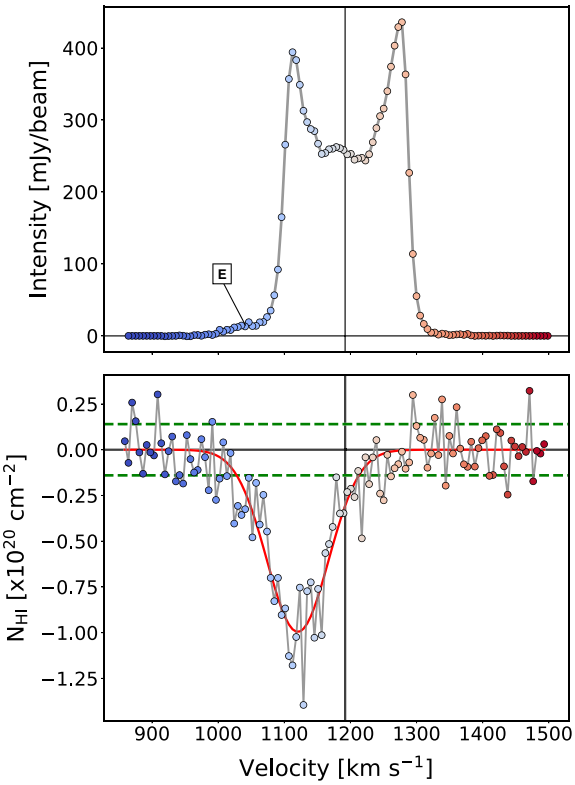


Figure 3. *Top panel:* NGC 5643 H I emission spectrum from the 30 arcsec cube. An asymmetry is observed between 1000 km s^{-1}and 1100 km s^{-1}, corresponding the northern H I tail (E). *Bottom panel:* H I absorption column density spectrum towards the centre of NGC 5643. The absorption spectrum was extracted from the central beam (diameter of 664 pc) of the 8 arcsec data cube. The average rms for the channels in the 8 arcsec cube is indicated by the horizontal green lines at $\pm 1.4 \times 10^{19}$ cm^{-2}. In both panels, the black vertical line represents the systemic velocity of the galaxy, $v_{\rm sys}$ = 1192 km s^{-1}.

however, a wing is present at blue-shifted velocities.The integrated flux of NGC 5643 with MeerKAT is $S_{\rm int}$ = 62.3 Jy/km s^{-1}, which suggests NGC 5643 is 10 per cent more H I massive than inferred in HIPASS. However a similar result was seen in de Blok et al. (2024), where they note that this discrepancy may be due to some H I emission being subtracted during the data processing, particularly when the bandpass correction method was applied. Another possible explanation is that the flux densities of H I bright sources in the HIPASS data may be affected by the gridding used in the HIPASS pipeline (de Blok et al. 2024). With MeerKAT, we are able to resolve the disc, as shown in the H I flux density distribution (moment 0) map (Fig. 4).

Fig. 4 shows the moment 0 map for the 30 arcsec cube, with 3σ and 9σ column density contours of the 96, 30, and 8 arcsec intensity map in cyan, green, and black, respectively. The H I is distributed in a circular disc with a 30 kpc diameter, highlighted in blue. The high column density gas within the disc traces the spiral arms well, highlighted in green and white.

The velocity field of NGC 5643 is shown in the top panel of Fig. 5 for the 30″ cube, revealing a regularly rotating H I disc with position angle, PA $\sim$ 315°. This is consistent with the PHANGS position angle (PA = 317°), measured from the rotation axis of the 13 kpc central molecular disc (Lang et al. 2020). The bottom panel of Fig. 5 presents the velocity dispersion map. The average velocity dispersion in the disc is $\sigma_{\rm v} \sim 20$ km s^{-1}. Around the edge of the

Downloaded from https://academic.oup.com/mnras/article/540/3/2396/8142523 by jamestemlett user on 14 August 2025

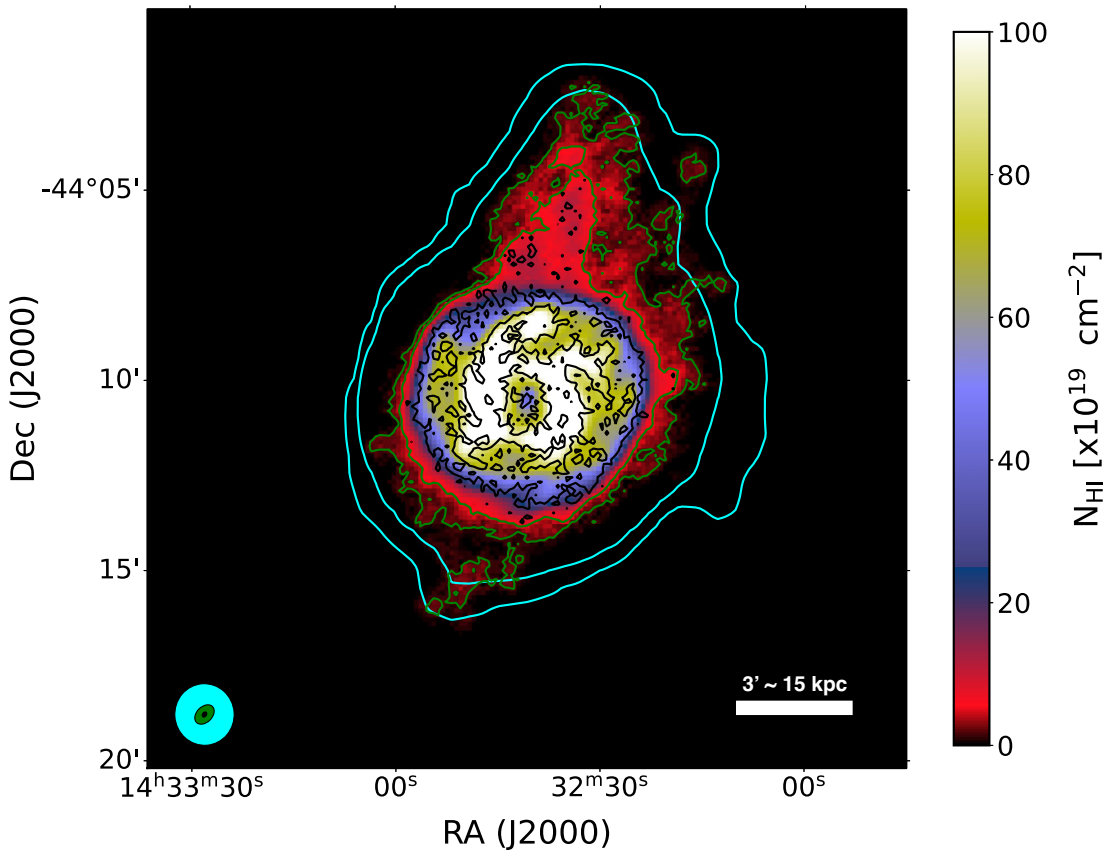


Figure 4. NGC 5643 intensity map for the 30″ cube with 3σ and 9σ H I column density contours for each cube. The 96 arcsec intensity map contour levels are [3.1, 9.3] $\times 10^{18}$ cm^{-2} (cyan). The 30 arcsec intensity map contour levels are [1.7, 5.2] $\times 10^{19}$ cm^{-2} (green). The 8″ intensity map contour levels are [2.9, 8.9] $\times 10^{20}$ cm^{-2} (black).

galactic disc, particularly in the northern and southern regions, we see higher velocity dispersions ($\geq$ 30 km s^{-1}), likely tracing more turbulent gas. This is similar to what is observed in NGC 2403, another nearby star-forming galaxy, where the velocity dispersion in the disc ranges from 8 to 12 km s^{-1}. In the central region and spiral arms of NGC 2403, the velocity dispersion reaches 10–15 km s^{-1}, producing a beard effect in the position velocity diagrams, which is linked to ongoing SF in these regions (see Sancisi et al. 2008; de Blok et al. 2014; Fraternali 2017). While the velocity dispersion in the anomalous infalling gas filament in NGC 2403 is higher, ranging from 20 to 50 km s^{-1} (see Fraternali et al. 2002; Veronese, de Blok & Walter 2023).

The most peculiar feature of the H I in NGC 5643 is the low-column density northern tail, which we detect in all data cubes. This tail extends $\sim$ 30 kpc from the nucleus of NGC 5643. Most of the tail has low column densities, ranging from 0.3–6 $\times$ 10^{19}cm^{-2}, and is most prominently observed in the 96 arcsec cube, even though it is resolved with only $\sim$ 2 beams. The tail is spatially resolved in the 30 arcsec data cube but only faintly visible in the 8 arcsec cube.

We study the channel maps of the 30 arcsec data cube, shown in Fig. 6, where the tail is visible between 1024 and 1200 km s^{-1}. This velocity range crosses the systemic velocity of the system. To further investigate, we create position velocity diagrams from the 30 arcsec data cube across different position angles (PA), as shown in Fig. 7. The cuts are made along the major rotation axis, PA = 315°, and along the tail feature, PA = 348°. The black contours corresponds to column densities of 2^n σ where n = 0, 1, 2, 3, with σ = 1.4 $\times$ 10^{19} cm^{-2}, the average column density at 3 SNR in the 30 arcsec cube over four channels of 5.5 km s^{-1}. The red contours at 2^n σ where n = $-$3, $-$2, $-$1, highlight the low column density features.

The majority of the H I gas is found in the star-forming disc of the galaxy, exhibiting regular rotation as shown by the almost symmetric rotation curves in the position velocity diagram along the major axis.

From the position velocity slice along the tail, we observe a stream of low column density emission extending beyond the systemic velocity (v_{sys} = 1192 km s^{-1}) and in the opposite direction to the gas in the H I disc, labelled as feature E. This extended feature corresponds to the northern part of the tail, which implies that the tail is counterrotating with respect to the H I disc. Additionally, the emission spectrum in Fig. 3 shows an asymmetry at blue-shifted velocities, which we now attribute to the northern tail feature.

This tail is not the only irregular gas in this galaxy. In the position velocity diagrams, we observe several asymmetries along the rotating disc. On the west side of the disc, between velocities of 1250 km s^{-1} and the systemic velocity (v_{sys} = 1192 km s^{-1}), the H I gas appears to be lagging, producing a beard feature, visible in both position velocity diagrams (feature C in Fig. 7). This beard feature is most likely caused by H I gas that has been expelled out of the main rotating disc due to galactic winds from supernovae activity (Sancisi et al. 2008; Fraternali 2017). This expelled H I gas is located out of the plane and is rotating more slowly than the disc (Schaap, Sancisi

Downloaded from https://academic.oup.com/mnras/article/540/3/2396/8142523 by jamestemlett user on 14 August 2025

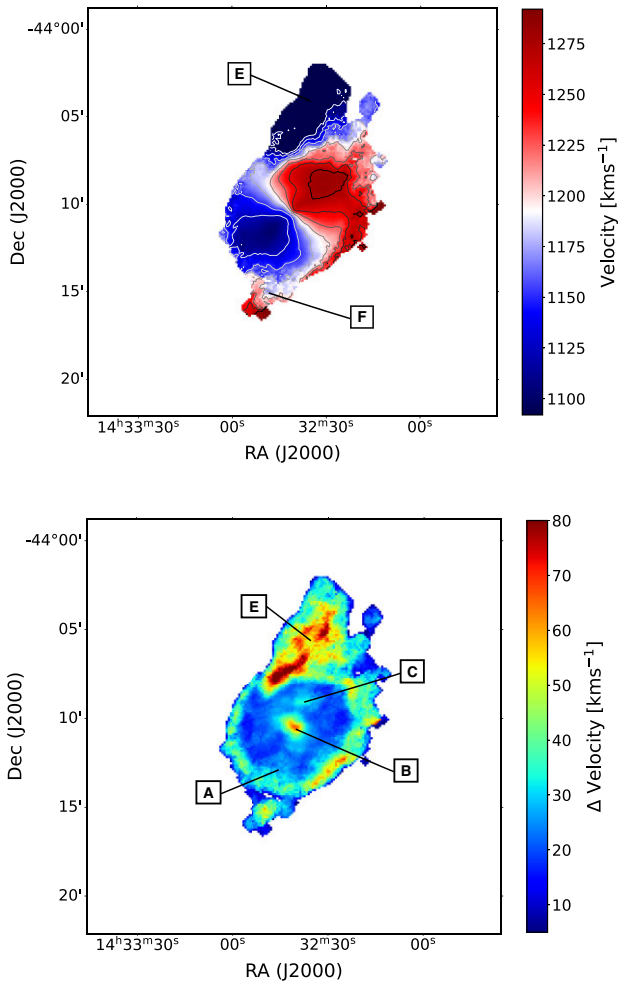


Figure 5. Kinematics of NGC 5643 from the 30 arcsec cube. *Top*: Velocity map (moment 1) centred on the systemic velocity of NGC 5643 (1192 km s^{-1}). The contours are from 1100 km s^{-1} to 1275 km s^{-1}, increasing in steps of 25 km s^{-1}. *Bottom*: Velocity dispersion map (moment 2) of NGC 5643. The annotations highlight features discussed throughout the paper.

& Swaters 2000). Further beard effects are seen in feature A at the blue-shifted velocities (1144–1166 km s^{-1}).

At the edge of the rotation curve, in the blue-shifted velocities, we observe diffuse gas sharply extending towards the systemic velocity, creating a hook effect, feature F, in Fig. 7. Feature F runs almost parallel to the northern tail and is associated with a smaller tail in the south of the disc, as seen in the velocity maps. These non-rotating features are discussed in more detail in Section 4.

3.3 H I Absorption

Until now, only H I emission had been detected in NGC 5643. Thanks to MeerKAT's sensitivity and resolution, we are now able to detect H I absorption against the continuum emission peak ($S_{1.4\,\mathrm{GHz}} \approx 18$ mJy beam^{-1}) in the nuclear region of NGC 5643, which was missed in the HIPASS survey. The H I absorption is not resolved along the weaker continuum emission of the bar and is detected in the central beam in the highest resolution data cube (8 arcsec). The H I absorption spectrum is shown in the bottom panel of Fig. 3, was extracted from the 8″ data cube, with the central beam corresponding to a diameter of 664 pc. The optical depth, τ, is calculated using the following equation (see e.g. Emonts et al. 2010):

$$e^{-\tau} = 1 - \frac{S_{\mathrm{abs}}}{S_{\mathrm{cont}}}, \tag{1}$$

where S_{abs} and S_{cont} are the absorption and continuum flux, respectively. We are then able to determine the column density of the H I absorption (e.g. Morganti & Oosterloo 2018):

$$N_{\mathrm{H\,I}}\,[\mathrm{cm}^{-2}] = 1.82 \times 10^{18}\, T_s[\mathrm{K}] \int \tau(v)\,\mathrm{d}v\ [\mathrm{km\,s}^{-1}]. \tag{2}$$

Assuming a spin temperature of $T_s = 100$ K, as commonly done for H I studies (see review from Morganti & Oosterloo 2018).

The peak absorbed flux, determined using a Gaussian fit profile, is $S_{\mathrm{abs}} \approx 2$ mJy beam^{-1}. This corresponds to an optical depth of $\tau \sim 0.1$ and a column density of approximately -1×10^{20} cm^{-2}. The full width at half-maximum (FWHM) of the line is 110 km s^{-1} ($\sim$ 20 channels).

In the bottom panel of Fig. 3, the absorption spectrum appears symmetric with a single peak that is slightly blue-shifted ($\Delta v \approx$72 km s^{-1}) relative to the systemic velocity of NGC 5643 ($v_{\mathrm{sys}} = 1192$ km s^{-1}), indicated by the vertical black line. The green horizontal dashed lines represent the average noise in the 8 arcsec cube. This absorption is also visible in the position velocity diagrams as feature B in Fig. 7, where its blue-shifted nature is evident.

The optical depths of the H I absorption line fall within the range typically associated with H I discs (see e.g. Gallimore et al. 1999; Maccagni et al. 2017). These values are significantly larger than those expected for H I outflows, which typically exhibit optical depths of $\tau \approx 0.01$ or less (see e.g. Morganti, Tadhunter & Oosterloo 2005; Geréb et al. 2015). The H I disc traced by the absorption is on the circum-nuclear kiloparsec scale, limited by the spatial resolution of 600 pc, and corresponds to the torus of the AGN which is the region outside the optically thick accretion disc typically found in nearby AGN (van Gorkom et al. 1989; Gallimore et al. 1999).

4 DISCUSSION

In this section, we examine the peculiar H I features revealed by the MeerKAT observations, including the tail, the high-velocity dispersion clouds in the star-forming disc and the H I absorption. We explore the possible origins of these features and their implications for the gas dynamics and evolutionary history of NGC 5643.

4.1 3D modelling of the H I disc kinematics

To gain further insight into the nature of the extended tail and beards, we analyse the H I kinematics in NGC 5643 using tilted ring modelling (e.g. Rogstad, Lockhart & Wright 1974). This is performed with `BBarolo`[3], a publicly available software package (Di Teodoro & Fraternali 2015).

The fitting was carried out in two stages. First, we defined initial values for the galaxy centre, systemic velocity (v_{sys}), rotational velocity (v_{rot}), inclination (i), and position angle (PA). These were based on the fit parameters from Alonso-Herrero et al. (2018), who modelled the ALMA molecular gas, as well as parameters from the `SoFiA-2` run. The molecular gas kinematics in the inner 655 pc of NGC 5643 were modelled by Alonso-Herrero et al. (2018) with PA = 320°, i = 35° and v_{sys} = 1198 km s^{-1} from Alonso-Herrero et al. (2018). For the initial H I disc model, we used inclination

[3]https://editeodoro.github.io/Bbarolo/

Downloaded from https://academic.oup.com/mnras/article/540/3/2396/8142523 by jamestemlett user on 14 August 2025

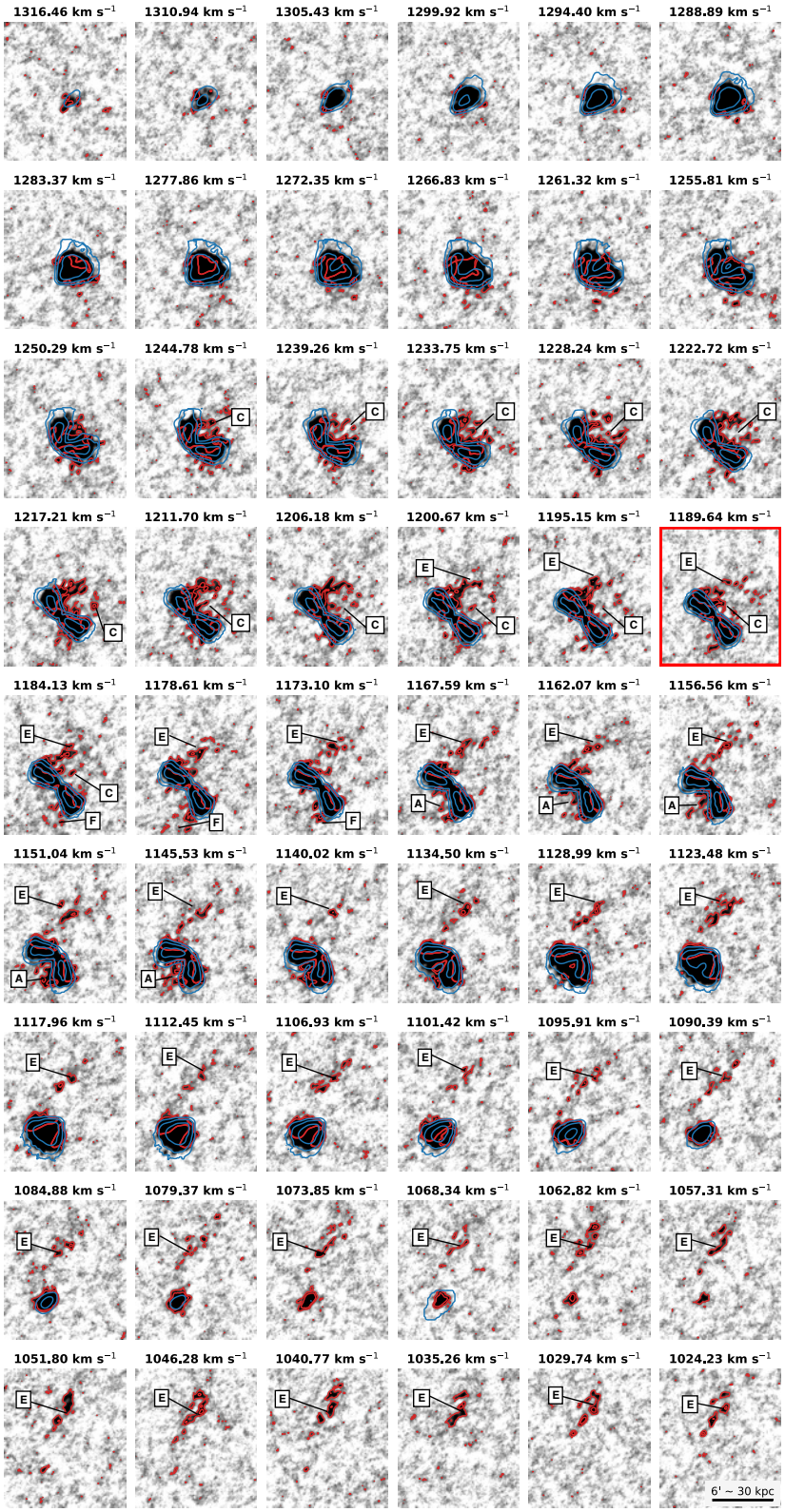


Figure 6. Channel maps of 30 arcsec cube, with the model (Section 4.1) in blue contours at [0.1, 1.0, 10] mJy beam^{-1}. The difference between the data and the model (the residual) is shown in red contours at [0.5, 1.0] mJy beam^{-1} isolating the tail and other non-rotating gas. The channel closest to the systemic velocity is marked with a red boarder. The labels provide an indication of the features discussed throughout the paper.

Downloaded from https://academic.oup.com/mnras/article/540/3/2396/8142523 by jamestemlett user on 14 August 2025

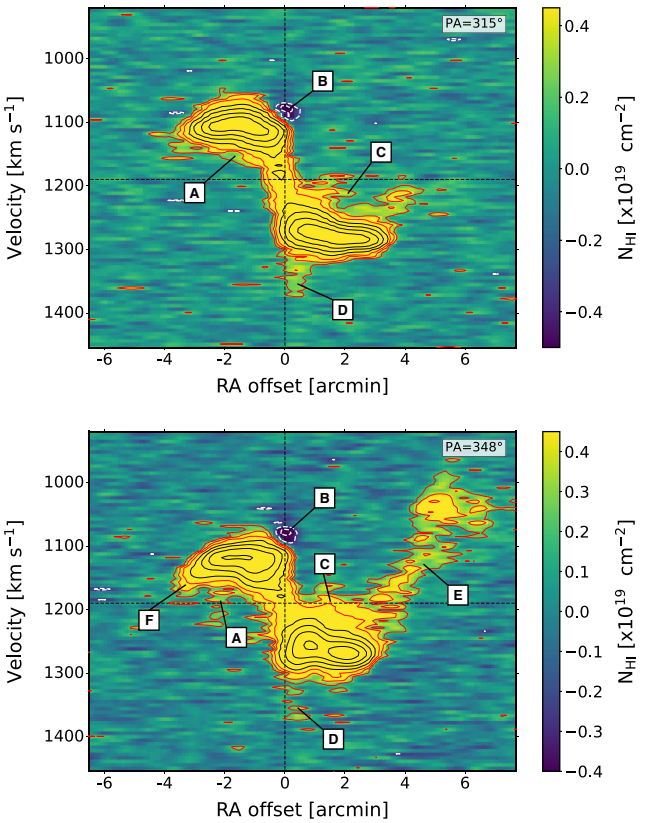


Figure 7. NGC 5643 position velocity diagrams. *Top panel:* Slice along the major rotation axis, PA = 315°. *bottom panel:* Slice along the tail feature, PA = 348°. Regions where SNR > 3 for the 30 arcsec cube are shown with black contours at column density levels of $2^n\sigma$ where $n = 0, 1, 2, 3$ and $\sigma = 1.4 \times 10^{19}$cm^{-2} over four channels. The red contours highlight the low column density features at $2^n\sigma$ where $n = -3, -2, -1$. White dashed contours at $[-0.5, -0.25] \times 10^{19}$ cm^{-2} indicate the H I absorption in the nuclear region of NGC 5643. The systemic velocity and centre of NGC 5643 are indicated by the black dashed horizontal and vertical lines, respectively. The annotations A –F highlight different features discussed throughout the paper.

$i = 35°$ as a free parameter, while PA = 308° and $v_{rot} = 120$ km s^{-1}were taken from the SoFiA-2 results. The systemic velocity was fixed at $v_{sys} = 1192$ km s^{-1}, also obtained from the SoFiA-2 run.

This process was repeated multiple times for each cube to optimize the model. Some parameters converged to a single value, while others were adjusted from free to fixed, specifically PA = 315°. The models derived from different cubes were consistent with each other. However, since the 30″ cube best captures both the asymmetric tails and beards without losing resolution, we utilize this model for further analysis. The final model consists of seven rings, with parameters listed in Table 4.

We present the fitted model over the H I emission per velocity channel in Fig. 6. The model provides a good fit to the H I disc; however, there is a noticeable amount of gas beyond the regions captured by the model, corresponding to features labelled in Fig. 7, suggesting complex gas flows in NGC 5643. These features are best highlighted in the position–velocity diagrams, where we compare the model (blue contours) with the observed data. Fig. 8 replicates the position velocity plots from Fig. 7 but includes the model for direct comparison.

Table 4. Rings comprising the Bbarolo model with $v_{sys} = 1192$ km s^{-1} and PA = 315° for each ring. The table provides the radius (R) in kpc and arcsec, as well as rotational velocity (v_{rot}) and inclination (i) for each ring.

R (kpc)	R (arcsec)	v_{rot} (km s^{-1})	i (deg)	S_{int} (mJy km s^{-1})
1	15	149	34	26.0
4	45	152	34	37.3
6	75	162	33	41.5
9	105	169	33	36.7
11	135	170	32	30.1
14	165	173	32	20.1
16	195	174	33	9.93

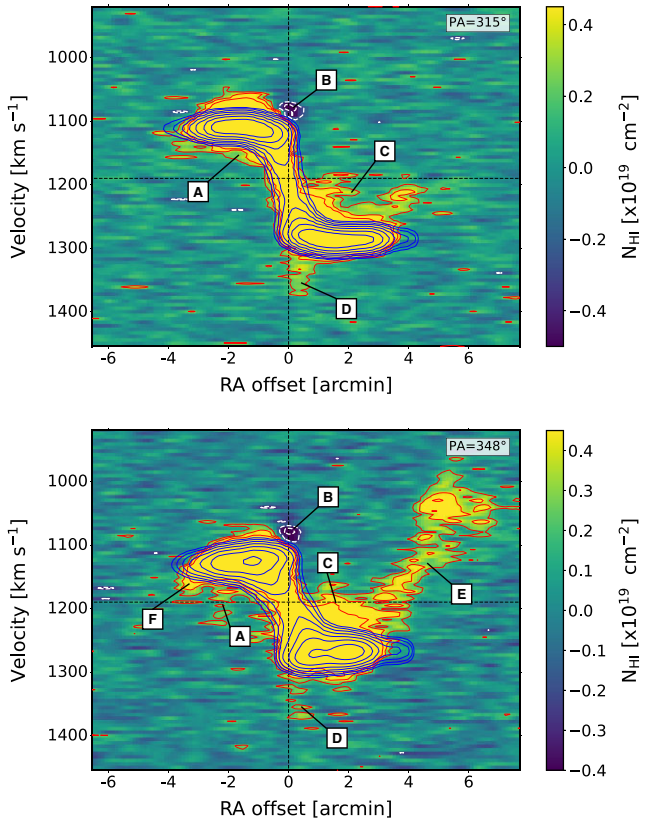


Figure 8. NGC 5643 position velocity diagrams, similar to Fig. 7, but with the model in blue contours at column density levels $2^n\sigma$ where $n \in (-3, 3)$ and $\sigma = 1.4 \times 10^{19}$cm^{-2}. As in Fig. 7, the low column density red contours are at $2^n\,\sigma$, where $n = -3, -2, -1$. The annotations A–F highlight different features discussed throughout the paper.

In Fig. 6, between 1145 and 1244 km s^{-1}, we observe gas lagging within the galactic disc. This lagging gas corresponds to the beards (Features A and C) seen in the position velocity diagrams (Fig. 8). The kinematics of the beards (C), described in Section 3.2, exhibit a significant deviation of $\sim$ 100 km s^{-1}, from the model. This deviation is comparable to the beards observed in NGC 2403, where gas deviates by 60–100 km s^{-1} from the main disc (de Blok et al. 2014). Another example is NGC 891, an edge-on galaxy, where H I is found as far as 22 kpc beyond the main disc and lags slightly behind the rotating H I disc (Oosterloo, Fraternali & Sancisi 2007). Oosterloo et al. (2007) suggest that this extended H I halo is primarily due to galactic fountains, though they do not rule out possible contributions

Downloaded from https://academic.oup.com/mnras/article/540/3/2396/8142523 by jamestemlett user on 14 August 2025

from intergalactic accretion in a filament at the outer edges of the disc.

The position velocity diagrams further reveal H I features in NGC 5643 that are not easily visible in the channel maps, such as Feature F, B, and D. Feature F corresponds to a small southern extension of H I, also seen in the velocity map (Fig. 5), likely resulting from H I stripping in PGC 538542. Feature B is the H I absorption seen against the continuum sources, while Feature D appears at the corresponding blue-shifted velocities from the H I absorption, suggesting that it may be H I located behind the continuum source.

Between 1024 and ∼1200 km s^{-1}, H I extends northward beyond the disc of NGC 5643, corresponding to the tail (feature E) in Figs 5 and 8. The tail feature exhibits significant asymmetry relative to the disc, with its associated H I gas counterrotating and extending beyond the galaxy's systemic velocity. The model allows us to predict the expected location of the gas in the outermost ring. However, the tail's velocity exceeds the expected rotational velocity by ∼ 250 km s^{-1}, further emphasizing the asymmetries disc's edge. Given this significant velocity deviation, it is unlikely that the cause of the beards linked to the cause of the tail feature.

To determine the mass of the tail feature, we subtracted the model from the data cube, producing a residual cube (shown as red contours in Fig. 6) and a corresponding residual intensity map. We then applied a 3σ clip and selected a box region to isolate the northern tail. After isolating the tail, we estimated its H I mass at $M_{\rm H\,I} \approx 4 \times 10^6$ M$_\odot$ corresponding to 0.1 per cent of the disc H I mass.

There are several possible explanations for the origin of this tail feature, including ram pressure stripping, recent interactions, or accretion from the environment. However, the kinematics of the tail, as seen in the position velocity plots and velocity (Figs 5 and 8), do not match the expected behaviour of ram pressure stripping. Serra et al. (2023) provide examples of ram pressure stripped galaxies in the Fornax cluster, where velocities smoothly extend from the galaxy's rotation and are dominated by its motion through the intracluster medium (ICM). In contrast, the tail in NGC 5643 exhibits counterrotation, inconsistent with this mechanism.

To further investigate whether the tail results from gas stripping, we assess whether NGC 5643 is H I deficient. Using the equations in Chung et al. (2009) and the mean H I surface density within the stellar disc, we calculate an H I deficiency of $\rm def_{H\,I} = -0.87 \pm 0.13$. According to the classification by Yoon et al. (2017), NGC 5643 falls into class 0, which includes galaxies that show no clear signs of gas stripping by the ICM. Instead, these galaxies are either symmetric and H I-rich or asymmetric with clear signs of tidal interactions. Therefore, the classification of NGC 5643 according to Yoon et al. (2017) and the H I deficiency does not indicate that gas is stripped off the galaxy.

The counterrotating kinematics of the tail suggest that it may be accreting on to NGC 5643, from various potential sources, such as a recent merger, a small tidally disrupted merging companion dwarf galaxy, or halo gas accretion from the environment. The tail in the north, along with the smaller tail in the south, may indicate ongoing tidal interaction. In the case of a recent massive merger event, we would expect the stars and gas in the system to be more disrupted and diffuse. However, in the disc of NGC 5643 the H I gas is regularly rotating, as seen in Fig. 5, and it follows the model well in the position velocity diagrams. Additionally, the deep optical image does not show stars being tidally stripped from the disc, with only an asymmetry in the upper spiral arms being observed.

While the asymmetries in H I emission in Fig. 2 may suggest an interaction between NGC 5643 and IC 4444, the two galaxies are spatially (234 kpc) and spectrally (758 km s^{-1}) distant from each other, and therefore not interacting. When compared to galaxy groups within 3500 km s^{-1} catalogue (Kourkchi & Tully 2017), NGC 5643 and IC 4444 are not identified as being part of the same group. Furthermore, there has been no evidence of large-scale filamentary structure prior to the discovery of these six H I sources.

In NGC 5643, it would take about two full rotations for the H I in the disc to settle into regular rotation (Struve et al. 2010). The time-scale for a full rotation is ∼ 0.7 Gyr, calculated using the $R_{\rm H\,I}$ = 16 kpc and $v_{\rm rot}$ = 150 km s^{-1}. This implies that the gas been settled for ∼ 1.4 Gyr. This time-scale does not align with what we would expect if NGC 5643 had recently undergone a major merger event.

In Section 3.1, we observed that NGC 5643 has more surrounding sources than previously thought, with seven H I sources (including IC 4444). The closest of these source, ID5, is located 104 kpc away and has an optical counterpart in the VST image. Assuming a typical velocity dispersion of ∼ 200 km s^{-1} in groups, with a dynamic mass of ∼ 24 × 10^{12} M$_\odot$ (see examples in Khosroshahi, Ponman & Jones 2007), the galaxies would have collided around ∼ 0.5 Gyrs ago, suggesting that no recent major interaction has occurred. The interaction time-scale of ID5 with NGC 5643 is close to the time-scale required for the gas in NGC 5643 to settle into regular rotation. Therefore, if ID5 is H I deficient, it is plausible that it may have passed close to NGC 5643 in a fly-by, losing H I gas that is now falling on to the more massive NGC 5643.

We also examined the VST image for any dwarf galaxies possibly associated with the northern tail. Due to NGC 5643 being close to the Galactic plane, the star density in the field of view is high, limiting the depth of our observations. Nonetheless, the surface brightness limit reached by these observations is comparable to that of the deepest optical surveys, such as VEGAS (∼ 27 mag arcsec^{-2}; Capaccioli et al. 2015) and DESI (∼ 22 mag arcsec^{-2}, Dey et al. 2019). There are several objects in the tail and edge of the galactic disc that could potentially be galaxies associated with NGC 5643 or in the background, but due to uncertainties in their redshifts, we cannot definitively confirm their association with NGC 5643.

Another possible interaction scenario is that a nearby dwarf galaxy was completely stripped by NGC 5643. In groups where recent interactions have occurred on massive galaxies, we expect to observe stellar streams connecting the stripped satellite galaxy and the main galaxy, as seen in the less dense environment of NGC 1316 (Iodice et al. 2017). However, the tail region of NGC 5643 appears to have a low stellar density and no visible stellar stream, making it unlikely that a disrupted galaxy is present within the tail.

The amount of H I in the tail is 4.6 × 10^6 M$_\odot$. If we very conservatively assume that the tidally stripped dwarf had a stellar mass equivalent to the H I in the tail, its corresponding apparent magnitude would be m = 20. Depending on its extent, this should be visible in the optical VST image, as discussed in Section 3.1. The VST image in Fig. 1, which includes H I continuum contours, reveals an increased concentration of light in the upper stellar spiral arm. This could indicate the presence of a dwarf galaxy embedded within the stellar disc of NGC 5643.

Additionally, diffuse H I emission is observed around the disc, including a small tail in the south, which could be linked to tidal features. In contrast, the northern tail is significantly larger (∼ 30 kpc), extending well beyond the disc, reaching a distance comparable to the galaxy's diameter. Currently, we lack metallicity measurements for the gas in the tail. Without this information, we cannot definitively determine whether the tail consists of pristine halo gas or originates from a stripped dwarf galaxy. If the tail resulted from

Downloaded from https://academic.oup.com/mnras/article/540/3/2396/8142523 by jamestemlett user on 14 August 2025

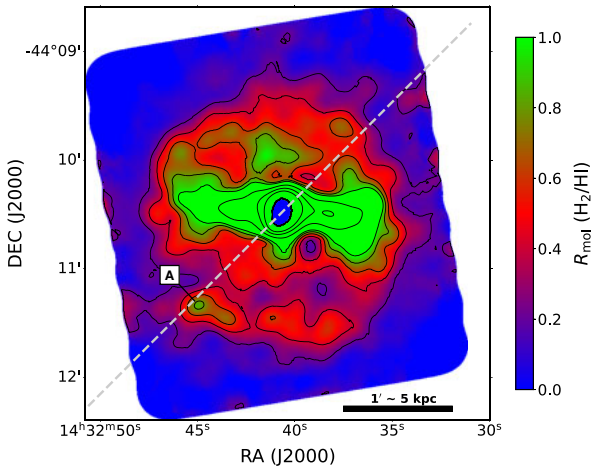


Figure 9. The spatial distribution of the H_2−to−H I ratio (R_{mol}) in NGC 5643 with contours at [0.2, 0.4, 0.6, 0.8, 1.0, 2.0, 4.0, 8.0]. The grey dashed line (PA = 315°) passes through the centre of NGC 5643 and represents the slice used for the position velocity diagram in Fig. 10. The 8 arcsec H I data were smoothed to 11 arcsec to match the resolution of the H_2 data for the R_{mol} comparison.

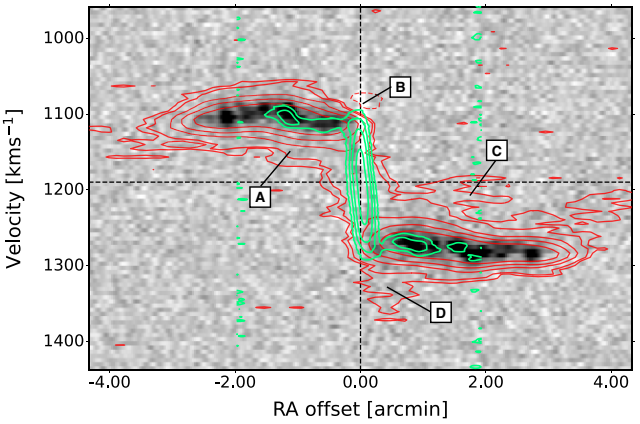


Figure 10. This position velocity diagram, slice along PA = 315°, comparing the H_2 and H I in inner 13 kpc of NGC 5643. The position velocity diagram for the 8 arcsec cube is shown in grey-scale, while the molecular hydrogen (H_2) is shown in green contours at [0.05, 0.125, 0.25, 0.5] K. The 30 arcsec H I cube is represented by red contours at [−0.8, 0.4, 0.8, 2.5, 5.0, 10.0] mJy beam^{-1}. The annotations correspond to the features seen in Fig. 8.

a disrupted dwarf, we would expect an increased stellar density in this region, accompanied by higher metallicity. Deep photometry from the VST data suggest a possible difference in stellar population in the radii of the tail (3–4 arcmin), as also indicted by the stellar population study in that region (Hoyt et al. 2021). Given these uncertainties, we cannot rule out the possibility that a small dwarf galaxy is associated with NGC 5643 and has been stripped.

The kinematics of the northern tail is unusual. It is counter-rotating with respect to the H I disc and extends beyond the systemic velocity of the galaxy by 200 km s^{-1}. The size and kinematics of the tail, along with the low H I deficiency in NGC 5643, lead us to believe that the tail is more likely H I associated with gas accreting from the environment. Given the tail's extent and low mass, it is possible that a dwarf galaxy either passed by, losing only its gas, or merged directly, contributing to the brighter features in the spiral arms. This suggests that the galaxy is actively accreting the counter-rotating H I gas, along with other non-rotating H I components in the south and at the galaxy's edge. Such gas inflows have predominantly been observed with molecular gas (see e.g. Combes et al. 2013, 2014; Davies et al. 2014) due to the sensitivity limit of previous telescopes. The improved sensitivity and resolution of MeerKAT observations are now beginning to reveal H I accretion in low-power AGN, such as Seyfert galaxies.

4.2 H_2 and H I comparison

To further analyse the H I disc, its beards and their connection with SF, we compare the H I and molecular hydrogen gas (H_2) distributions. We make use of the ALMA CO(2–1) line observations, as mentioned in Section 2.4. To determine the mass of the H_2 traced by the CO(2–1), Leroy et al. (2021) assumes a standard Milky Way conversion factor of $\alpha_{CO} = 4.35\,M_\odot\,pc^{-2}\,(K\ km\ s^{-1})^{-1}$, which is appropriate for this galaxy type, and CO(2–1) - to - CO(1–0) line ratio $R_{21} = 0.65$. The resulting H_2 mass is thus calculated to be $\log(\frac{M_{H_2}}{M_\odot}) = 9.4$.

We estimate the SFE of NGC 5643 using the ratio between H_2 and H I surface densities, defined as $R_{mol} = \sum_{H_2} / \sum_{H\,I}$, since SFE $\propto R_{mol}$ (Leroy et al. 2008). Using the available multiwavelength data, we created a map of R_{mol} (Fig. 9) by smoothing the 8 arcsec MeerKAT intensity map to match the 11 arcsec resolution of the ALMA map. Regions where $R_{mol} < 1$ correspond to areas where the H I mass exceeds the H_2 mass. In contrast, regions with $R_{mol} \geq 1$, where H_2 is dominant, are located along the bar and associated with star-forming regions, as indicated by the continuum image in Fig. 1. Along the bar, R_{mol} remains nearly constant, suggesting efficient SF. Leroy et al. (2008) examined the SFE as a function of radius for 23 nearby galaxies and found that nuclear regions exhibit a flat R_{mol}, indicative of efficient SF. Our results with NGC 5643 are consistent with their findings, as expected.

The regions north of the bar exhibit higher R_{mol} ($R_{mol} > 0.5$) than those south of the bar, except for a few bright-spots in the south. These regions, which presumably have higher SF activity, may be expelling gas out of the disc and could thus be responsible for the beards (A and C) observed in the position velocity diagrams in Fig. 8.

We investigate the kinematics of the southern bright-spots, where $R_{mol} > 0.5$, using a position velocity map for the ALMA CO(2–1) PHANGS data. The slice is taken across the centre of NGC 5643 at PA = 315°, intersecting the leftmost bright-spot. The molecular gas position velocity diagram (green) is overlaid on the 8 arcsec position velocity diagram (grey-scale) at the same slice, shown in Fig. 10. The red contours represent the 30 arcsec position velocity diagram along the same slice.

In the high-resolution (8 arcsec) H I position velocity diagram, we observe that the molecular and neutral atomic phases are linked and exhibit similar kinematics. At ∼ 1100 km s^{-1}, an increase in both H I and H_2 is associated with the leftmost bright-spot and feature A. Given the high spectral resolution of our data, we are able to resolve this elongation, which extends out to 1150 km s^{-1}, confirming that it is H I that has been blown out and is less dense than the H_2. These bright-spots lie along a spiral arm, where high SF rates are expected to expel both atomic and molecular gas out of the galactic plane. The kinematics associated with the bright-spot confirm ongoing SF and gas recycling in the spiral arms.

Having a complete picture of the molecular and atomic gas phases of the interstellar medium (ISM) in NGC 5643, we investigate whether NGC 5643 possesses a sufficiently large gas reservoir to sustain ongoing SF. SFE, which is proportional to R_{mol}, is inversely

Downloaded from https://academic.oup.com/mnras/article/540/3/2396/8142523 by jamestemlett user on 14 August 2025

proportional to the depletion time (t_{dep}); the time required for current SF to consume the available gas reservoir (Leroy et al. 2008). Using the H I mass derived from these observations and the H_2 gas mass from PHANGS, $\log(\frac{M_{H_2}}{M_\odot}) = 9.4$, we calculate the H I depletion time to be $t_{dep}(H\,I) \approx 1.79$ Gyrs and the total gas depletion time to be $t_{dep}\,(H\,I + H_2) \approx 3.74$ Gyr, using equations from Jaskot et al. (2015). This short depletion time suggests that the galaxy needs to be replenished with cold gas to sustain the ongoing SF. The accreting H I tail from the IGM, either as a remnant of a tidal interaction or directly from the halo, may contribute to this refuelling.

4.3 Nuclear region of NGC 5643

The active circum-nuclear region of NGC 5643 has been extensively studied in molecular and ionized gas (Cresci et al. 2015; Alonso-Herrero et al. 2018; Mingozzi et al. 2019; Venturi et al. 2021). 8.4 GHz continuum observations with the VLA by Leipski et al. (2006) reveal that NGC 5643 hosts weakly collimated radio jets, approximately 30 arcsec (2.5 kpc) in diameter long, extending on both sides of the nucleus along an east–west jet axis. Using the MUSE instrument, Cresci et al. (2015) report a bipolar ionization cone parallel to the jets surrounding the AGN. These ionization cones extend beyond 1.2 kpc on either side, aligned with the radio jets. At the centre of these cones, blue-shifted out-flowing ionized gas is observed, with projected velocity $v \sim -450$ km s^{-1}. There is also a possibility of a smaller jet structure in the same direction as the outer jets, which may have cleared out the molecular gas from the inner regions. This is suggested by Alonso-Herrero et al. (2018), who report a region of cleared molecular gas approximately 1 kpc from the AGN, based on ALMA observations.

As shown in Fig. 3, the H I absorption is symmetric and blue-shifted by 72 km s^{-1}. This small shift is unlikely to be tracing the outflow, which in the molecular and ionized phase is observed at $\sim$ 189 and $\sim$ 750 km s^{-1}, respectively (García-Bernete et al. 2021).

The absorption feature is also observed in the position velocity diagrams (feature B), where, at the corresponding red-shifted velocities, H I appears in emission (feature D). This could trace the gas behind the nucleus, while the absorption traces the gas in front. Given that these two features are seen at symmetric velocities with respect to the systemic velocity, it is likely that the absorption is simply tracing the gas in the innermost regions, which are regularly rotating within the bar. The H I tail that is fuelling the rotating disc may also contribute the nuclear activity through the secular motions of the bar.

Venturi et al. (2021) report high [O III] velocity dispersion perpendicular to the main radio jets. This perpendicular component is $\sim$ 3 kpc in length. Since the radio jets are low-powered ($\lesssim 10^{44}$erg s^{-1}), Venturi et al. (2021) suggest that the jet interacts with the ISM, creating this high-velocity dispersion region perpendicular to the jet. We do not see these perpendicular outflows in H I but instead find a deficit of H I in the regions perpendicular to the jets. This also accounts for the increase in R_{mol} perpendicular to the bar in the southerly direction, as seen in the R_{mol} map in Fig. 9. This may suggest that the jets are ionizing the gas, initially acting on the H I and then destroying the remaining dense molecular clouds.

VLBI observations will be valuable for understand the nature of the absorption, particularly in determining whether it is associated with jet outflows. Sub-kpc scale angular resolution will enable us to resolve the jets and the H I absorption, providing new insights into the location of this gas within the circum-nuclear regions both spatially and spectrally.

5 SUMMARY AND CONCLUSIONS

We present MeerKAT neutral hydrogen intensity and kinematic maps of the nearby spiral galaxy NGC 5643 and its surroundings. MeerKAT resolves both diffuse and small-scale structures of NGC 5643, providing unique insights spanning from circumgalactic to circum-nuclear scales. We also presented VST optical observations and compare the H I distribution with the H_2 emission from ALMA observations.

Surrounding NGC 5643 in the 1.5 deg^2 field of view, we identify new H I sources. Excluding IC 4444, this is the first detection of these sources in H I and, therefore, the first time their spectroscopic redshifts have been determined. We compared the H I sources to the optical VST image and found optical counterparts for ID4, ID5 and ID6. These sources have an H I mass $M_{H\,I} \approx 3 \times 10^7$ M$_\odot$. The closest source, ID5, has a projected spatial separation of 104 kpc and is too distant to have had a recent major interaction with NGC 5643 as the age for the latest possible major interaction is $\sim$ 1.2 Gyr.

While these MeerKAT observations were limited to a single pointing, the discovery of these six lower mass NGC 5643 neighbours, combined with previous analyses, suggests this is likely a small group. Future Square Kilometre Array (SKA) observations and wide-field surveys will provide a complete view of these types of gas structures.

In NGC 5643, the H I emission follows the star-forming spiral arms in a regularly rotating disc with $v_{rot} = 150$ km s^{-1} and major rotation axis PA = 315°. Given that the disc is regularly rotating to its outermost radius of 16 kpc, the last major interaction that may have unsettled the gas disc kinematics probably occurred $\gtrsim$ 1 Gyr ago. We find small gaseous clouds with low column density (3×10^{18}cm^{-2}) gas that is associated with NGC 5643 but not regularly rotating within the disc. These clouds, seen as lagging gas (beards) in the position velocity diagrams, have likely been expelled from the disc due to ongoing SF.

The H_2 and H I comparison of the inner 13 kpc in NGC 5643 reveals regions of increased SFE, which correspond to the beards in the position velocity diagrams. North and south of the bar, there are also regions of increased H_2 that spatially coincide with the spiral arms, with kinematics matching those of the beards seen in H I. The H I depletion time calculated from SFE is $t_{dep}(H\,I) \approx 1.8$ Gyr. For the ongoing SF the cold gas in this galaxy needs to be refuelled by accreting IGM, either from the remnant of a tidal interaction or directly from the halo.

The most noticeable low column density feature in NGC 5643 is a diffuse northern tail extending out to 30 kpc and counter-rotating with respect to the H I disc. This is the first time the tail of diffuse H I ($\sim 4 \times 10^6$ M$_\odot$) has been observed to such an extent and resolution. The H I deficiency of NGC 5643 is low, $def_{H\,I} = -0.87 \pm 0.13$, indicating that the H I is not being stripped from the galaxy (Yoon et al. 2017). The kinematics also do not match what we would expect in a ram pressure stripped galaxy.

This H I accreting on to the galaxy is either from the halo or due to a dwarf galaxy that has been stripped by NGC 5643. In the optical VST image of NGC 5643, this dwarf galaxy is not visible in the H I tail but may be embedded in the face-on stellar disc, as suggested by a bump in one of the upper stellar arms.

The tail's peculiar kinematics, which extends beyond the systemic velocity of the galaxy, suggest that if the tail belonged to a dwarf galaxy, its stellar body (with a mass of 10^4–10^6 M$_\odot$) should have been visible in the deep optical image, since the tail has a H I mass of $M_{H\,I} = 5.4 \times 10^6$. More information on the other phases of this

Downloaded from https://academic.oup.com/mnras/article/540/3/2396/8142523 by jamestemlett user on 14 August 2025

gaseous tail and its metallicity would provide new insights into constraining its nature.

H I absorption is detected in NGC 5643 against a continuum source. The absorption feature is slightly blue-shifted ($\Delta v \approx -72$ km s^{-1}) with a small H I emission counterpart at higher velocities. This symmetry is due to the bar feature, with gas in front of the continuum source (absorption) and the gas behind the continuum source (H I emission at corresponding, but positive velocity). The H I tail is fuelling the rotating disc, and through the secular motions of the bar, part of this gas may also fuel the nuclear activity.

We conclude that the neutral hydrogen MeerKAT observation of NGC 5643 has resolved an extended northern tail with anomalous kinematics for the first time. Our results demonstrate that this tail represents the accretion of H I onto a regularly rotating H I disc. While we cannot definitively determine the origin of this H I accretion, it may be the result of a stripped dwarf galaxy or simply H I in the environment of NGC 5643. Ongoing SF can be observed in both H I emission and in H I to H_2 comparisons. The H I absorption feature provides insight into the sub-kpc nuclear region of NGC 5643; however, a more in-depth study of the central 1 kpc is required to fully understand the physical process occurring around the AGN.

These new results provide a more holistic view of NGC 5643. MeerKAT observations, such as this one, with high resolution and sensitivity, allow us to gain a more complete understanding of galaxies and how they are formed, evolved and sustained. As MeerKAT transitions to the SKA, studies such as this will be possible at higher redshifts, making local case studies important examples for broader cosmological research.

ACKNOWLEDGEMENTS

The authors thank the anonymous referee for the useful comments and suggestions that helped improve the paper.

The authors would also like to thank Dr G. Venturi for the helpful discussions and suggestions.

KCS and RPD hereby acknowledge the financial assistance of the South African Radio Astronomy Observatory (SARAO, www.sarao.ac.za), which is a facility of the National Research Foundation (NRF), an agency of the Department of Science and Innovation (DSI). RPD's research is funded by the South African Research Chairs Initiative of the Department of Science, Technology, and Innovation; and the National Research Foundation (Grant ID: 77948). KCS acknowledges financial support from the South African Department of Science and Innovation's National Research Foundation under the Italy-South Africa Joint Research Programme (ISARP) RADIOMAP Joint Research Scheme (DSI-NRF Grant Number 150551).

JH acknowledges support from the UK SKA Regional Centre (UKSRC). The UKSRC is a collaboration between the University of Cambridge, University of Edinburgh, Durham University, University of Hertfordshire, University of Manchester, University College London, and the UK Research and Innovation (UKRI) Science and Technology Facilities Council (STFC) Scientific Computing at the Rutherford Appleton Laboratory (RAL). The UKSRC is supported by funding from the UKRI STFC.

Part of the research activities described in this paper were carried out with contribution of the Next Generation EU funds within the National Recovery and Resilience Plan (PNRR), Mission 4 – Education and Research, Component 2 – From Research to Business (M4C2), Investment Line 3.1 – Strengthening and creation of Research Infrastructures, Project IR0000034 – 'STILES – Strengthening the Italian Leadership in ELT and SKA'.

This work has received funding from the European Research Council (ERC) under the European Union's Horizon 2020 research and innovation programme (grant agreement no. 882793 'MeerGas').

The MeerKAT telescope is operated by the South African Radio Astronomy Observatory, which is a facility of the National Research Foundation, an agency of the Department of Science, Technology, and Innovation. Part of the research is based on data collected with the INAF VST telescope at the ESO Paranal Observatory.

Part of the data published here have been reduced using the Containerized Automated Radio Astronomy Calibration (CARACal) pipeline, partially supported by ERC Starting grant number 679627 'FORNAX', MAECI Grant Number ZA18GR02, DST-NRF Grant Number 113121 as part of the ISARP Joint Research Scheme, and BMBF project 05A17PC2 for D-MeerKAT. Information about CARACal can be obtained online under the URL: https://caracal.readthedocs.io.

We acknowledge the use of the ilifu cloud computing facility – www.ilifu.ac.za, a partnership between the University of Cape Town (UCT), the University of the Western Cape, Stellenbosch University, Sol Plaatje University, the Cape Peninsula University of Technology and the South African Radio Astronomy Observatory. The ilifu facility is supported by contributions from the Inter-University Institute for Data Intensive Astronomy (IDIA – a partnership between the University of Cape Town, the University of Pretoria and the University of the Western Cape), the Computational Biology division at UCT and the Data Intensive Research Initiative of South Africa (DIRISA). This work made use of the CARTA (Cube Analysis and Rendering Tool for Astronomy) software (DOI 10.5281/zenodo.3377984 – https://cartavis.github.io).

DATA AVAILABILITY

The raw visibilities used in this work can be found at the SARAO archive[4] The authors may make data products available upon reasonable request.

REFERENCES

Alonso-Herrero A. et al., 2018, ApJ, 859, 144
Barnes D. G. et al., 2001, MNRAS, 322, 486
Best P. N., Heckman T. M., 2012, MNRAS, 421, 1569
Capaccioli M. et al., 2015, A&A, 581, A10
Carignan C., Libert Y., Lucero D. M., Randriamampandry T. H., Jarrett T. H., Oosterloo T. A., Tollerud E. J., 2016, A&A, 587, L3
Chung A., van Gorkom J. H., Kenney J. D. P., Crowl H., Vollmer B., 2009, AJ, 138, 1741
Combes F. et al., 2013, A&A, 558, A124
Combes F. et al., 2014, A&A, 565, A97
Cresci G. et al., 2015, A&A, 582, A63
Dasyra K. M., Combes F., Oosterloo T., Oonk J. B. R., Morganti R., Salomé P., Vlahakis N., 2016, A&A, 595, L7
Davies R. I. et al., 2014, ApJ, 792, 101
de Blok W. J. G. et al., 2014, A&A, 569, A68
de Blok W. J. G. et al., 2024, A&A, 688, A109
Dey A. et al., 2019, AJ, 157, 168
Di Teodoro E. M., Fraternali F., 2015, MNRAS, 451, 3021
Ellison S. L., Catinella B., Cortese L., 2018, MNRAS, 478, 3447
Emonts B. H. C. et al., 2010, MNRAS, 406, 987
Fraternali F., 2017, in Fox A., Davé R., eds, Astrophysics and Space Science Library, Vol. 430, Gas Accretion onto Galaxies. Springer, Cham, p. 323
Fraternali F., van Moorsel G., Sancisi R., Oosterloo T., 2002, AJ, 123, 3124

[4]https://archive.sarao.ac.za

Downloaded from https://academic.oup.com/mnras/article/540/3/2396/8142523 by jamestemlett user on 14 August 2025

Gallimore J. F., Baum S. A., O'Dea C. P., Pedlar A., Brinks E., 1999, ApJ, 524, 684
García-Bernete I. et al., 2021, A&A, 645, A21
Geréb K., Maccagni F. M., Morganti R., Oosterloo T. A., 2015, A&A, 575, A44
Harrison C. M., Costa T., Tadhunter C. N., Flütsch A., Kakkad D., Perna M., Vietri G., 2018, Nat. Astron., 2, 198
Heald G. et al., 2016, MNRAS, 462, 1238
Hess K. M., Jarrett T. H., Carignan C., Passmoor S. S., Goedhart S., 2015, MNRAS, 452, 1617
Hopkins P. F., Hernquist L., Cox T. J., Di Matteo T., Martini P., Robertson B., Springel V., 2005, ApJ, 630, 705
Hopkins P. F., Torrey P., Faucher-Giguère C.-A., Quataert E., Murray N., 2016, MNRAS, 458, 816
Hoyt T. J. et al., 2021, ApJ, 915, 34
Ianjamasimanana R. et al., 2022, MNRAS, 513, 2019
Iodice E. et al., 2016, ApJ, 820, 42
Iodice E. et al., 2017, ApJ, 839, 21
Jaskot A. E., Oey M. S., Salzer J. J., Van Sistine A., Bell E. F., Haynes M. P., 2015, ApJ, 808, 66
Jones D. H. et al., 2009, MNRAS, 399, 683
Józsa G. I. G. et al., 2020, ASP Conf. Ser. Vol. 527, Astronomical Data Analysis Software and Systems XXIX. Astron. Soc. Pac., San Francisco, p. 635
Kenyon J. S., Smirnov O. M., Grobler T. L., Perkins S. J., 2018, MNRAS, 478, 2399
Kereš D., Katz N., Weinberg D. H., Davé R., 2005, MNRAS, 363, 2
Khosroshahi H. G., Ponman T. J., Jones L. R., 2007, MNRAS, 377, 595
Kleiner D. et al., 2021, A&A, 648, A32
Koribalski B. S. et al., 2004, AJ, 128, 16
Kormendy J., Kennicutt Robert C. J., 2004, ARA&A, 42, 603
Kourkchi E., Tully R. B., 2017, ApJ, 843, 16
Lang P. et al., 2020, ApJ, 897, 122
Leipski C., Falcke H., Bennert N., Hüttemeister S., 2006, A&A, 455, 161
Leroy A. K. et al., 2021, ApJS, 257, 43
Leroy A. K., Walter F., Brinks E., Bigiel F., de Blok W. J. G., Madore B., Thornley M. D., 2008, AJ, 136, 2782
Maccagni F. M. et al., 2020, A&A, 634, A9
Maccagni F. M. et al., 2021, A&A, 656, A45
Maccagni F. M. et al., 2023, A&A, 675, A59
Maccagni F. M. et al., 2024, A&A, 690, A69
Maccagni F. M., Morganti R., Oosterloo T. A., Geréb K., Maddox N., 2017, A&A, 604, A43
Maccagni F., Morganti R., Oosterloo T., Mahony E., 2014, A&A, 571, A67
Meyer M. J. et al., 2004, MNRAS, 350, 1195
Mingozzi M. et al., 2019, A&A, 622, A146
Morganti R., Frieswijk W., Oonk R. J. B., Oosterloo T., Tadhunter C., 2013, A&A, 552, L4
Morganti R., Oosterloo T., 2018, A&A Rev., 26, 4
Morganti R., Oosterloo T., Oonk J. B. R., Frieswijk W., Tadhunter C., 2015, A&A, 580, A1
Morganti R., Oosterloo T., Tsvetanov Z., 1998, AJ, 115, 915
Morganti R., Peck A. B., Oosterloo T. A., van Moorsel G., Capetti A., Fanti R., Parma P., de Ruiter H. R., 2009, A&A, 505, 559
Morganti R., Tadhunter C. N., Oosterloo T. A., 2005, A&A, 444, L9
Morris S., Ward M., Whittle M., Wilson A. S., Taylor K., 1985, MNRAS, 216, 193
Namumba B. et al., 2021, MNRAS, 505, 3795
Offringa A. R. et al., 2014, MNRAS, 444, 606
Offringa A. R., van de Gronde J. J., Roerdink J. B. T. M., 2012, A&A, 539, A95
Oosterloo T. A., Morganti R., Tzioumis A., Reynolds J., King E., McCulloch P., Tsvetanov Z., 2000, AJ, 119, 2085
Oosterloo T., Fraternali F., Sancisi R., 2007, AJ, 134, 1019
Pan H.-A. et al., 2022, ApJ, 927, 9
Péroux C., Howk J. C., 2020, ARA&A, 58, 363
Poggianti B. M. et al., 2017, Nature, 548, 304
Poggianti B. M., GASP Team, 2023, Proc. IAU Symp. 373, Resolving the Rise and Fall of Star Formation in Galaxies. p. 163
Press W. H., Schechter P., 1974, ApJ, 187, 425
Radovich M., Poggianti B., Jaffé Y. L., Moretti A., Bettoni D., Gullieuszik M., Vulcani B., Fritz J., 2019, MNRAS, 486, 486
Rodríguez Montero F., Davé R., Wild V., Anglés-Alcázar D., Narayanan D., 2019, MNRAS, 490, 2139
Rogstad D. H., Lockhart I. A., Wright M. C. H., 1974, ApJ, 193, 309
Salomé Q., Salomé P., Miville-Deschênes M. A., Combes F., Hamer S., 2017, A&A, 608, A98
Sancisi R., Fraternali F., Oosterloo T., van der Hulst T., 2008, A&AR, 15, 189
Santoro F., Oonk J. B. R., Morganti R., Oosterloo T. A., Tadhunter C., 2016, A&A, 590, A37
Schaap W. E., Sancisi R., Swaters R. A., 2000, A&A, 356, L49
Serra P. et al., 2023, A&A, 673, A146
Spavone M. et al., 2017, A&A, 603, A38
Struve C., Oosterloo T. A., Morganti R., Saripalli L., 2010, A&A, 515, A67
Stuber S. K. et al., 2023, A&A, 676, A113
van Gorkom J. H., Knapp G. R., Ekers R. D., Ekers D. D., Laing R. A., Polk K. S., 1989, AJ, 97, 708
Venhola A. et al., 2019, A&A, 625, A143
Venturi G. et al., 2021, A&A, 648, A17
Veronese S., de Blok W. J. G., Walter F., 2023, A&A, 672, A55
Watkins E. J. et al., 2023, A&A, 676, A67
Westmeier T. et al., 2021, MNRAS, 506, 3962
Yoon H., Chung A., Smith R., Jaffé Y. L., 2017, ApJ, 838, 81

APPENDIX A: H I SOURCES SURROUNDING NGC 5643

As mentioned in Section 2 there are seven H I sources surrounding NGC 5643 (Fig. 2), six of which are new detection. In this section, we present additional results for these sources. Fig. A1 displays optical images with H I intensity contours, velocity maps, velocity dispersion maps and H I spectra for each source. The contour levels are stated in each image. The arrow on the velocity map indicates the major rotation axis as determined by `SoFiA-2`. These figures were generated using the `SoFiA-2` Imaging Pipeline (SIP).[5]

[5]https://github.com/kmhess/SoFiA-image-pipeline

Downloaded from https://academic.oup.com/mnras/article/540/3/2396/8142523 by jamestemlett user on 14 August 2025

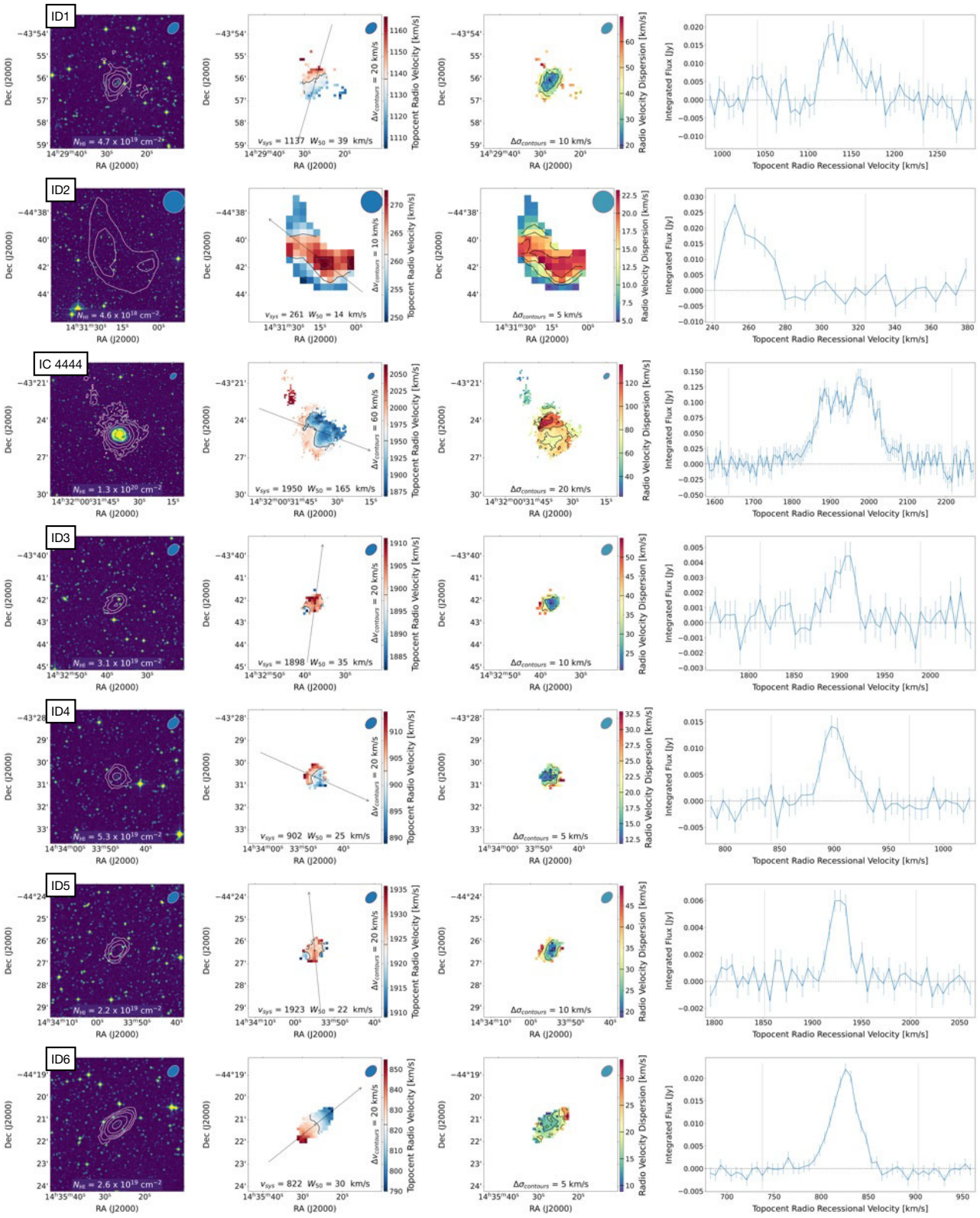


Figure A1. The H I sources surrounding NGC 5643. From left to right (i): Optical Digitized Sky Survey (DSS) images with primary beam-corrected H I column density contours. The contour levels follow $2^n \times N_{\rm H\,I}$ (with $n = 0, 1, ...$), where the base H I column density values, $N_{\rm H\,I}$, are shown at the bottom of each image. (ii) Intensity-weighted velocity field. The arrow indicates the major rotation axis as determined by `SoFiA-2` and the black contour marks the systemic velocity of the source. (iii) Velocity dispersion map. (iv) H I emission spectra with noise. The vertical lines enclose the channel range of the H I emission. For (i), (ii), and (iii) the contour levels are provided on each image, and the beam shown in the top right. These images are derived from the 30 arcsec cube, except for ID2, which is only visible in the 96 arcsec cube.

Downloaded from https://academic.oup.com/mnras/article/540/3/2396/8142523 by jamestemlett user on 14 August 2025

APPENDIX B: RING PROPERTIES OF NGC 5643.

In Section 4.1, we described the generation a model for the H I disc in NGC 5643 using `Bbarolo` with the 30 arcsec cube. The rotational velocity (V_{rot}) was treated as a free parameter when running the `Bbarolo` fitting. The top panel of Fig. B1 shows how this parameter changes with each ring in the model. The errors in V_{rot} were calculated by taking 5 per cent of the value and adding the channel resolution, 5.5 km s^{-1}.

The bottom panel of Fig. B1 shows the H I flux density per ring with the standard deviation, as determined by `Bbarolo`. We observe an increase in flux density up to 7 kpc, followed by a decreases towards the outer edge of the disc. A decline in H I is noted towards the centre of NGC 5643, which can be attributed to the H I absorption discussed in Section 4.3. The model terminates at the disc's edge and does not account for the northern tail.

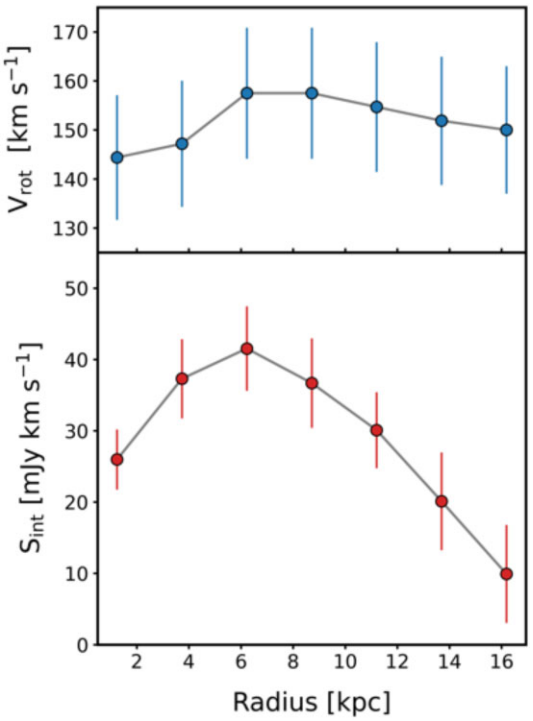


Figure B1. *Top panel:* Rotational velocity plot for each ring in the model. The error bars are 5 per cent of the value added to the channel resolution of 5.5 km s^{-1}. *Bottom panel:* H I flux density per ring. These results are from the tilted-ring model fitting performed with `Bbarolo` on the 30 arcsec cube. The error bars are the standard deviation values as determined by `Bbarolo`.

This paper has been typeset from a TEX/LATEX file prepared by the author.

Downloaded from https://academic.oup.com/mnras/article/540/3/2396/8142523 by jamestemlett user on 14 August 2025

© 2025 The Author(s).
Published by Oxford University Press on behalf of Royal Astronomical Society. This is an Open Access article distributed under the terms of the Creative Commons Attribution License (https://creativecommons.org/licenses/by/4.0/), which permits unrestricted reuse, distribution, and reproduction in any medium, provided the original work is properly cited.